2-8-2011

Optimization of a Terahertz Radiator
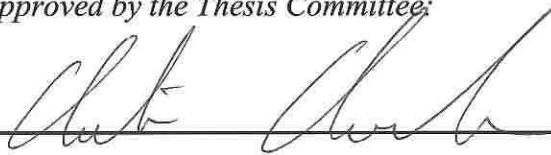
Douglas Brown

Douglas G Brown
Candidate

Electrical and Computer Engineering
Department

This thesis is approved, and it is acceptable in quality
and form for publication:

Approved by the Thesis Committee:

, Chairperson

OPTIMIZATION OF A TERAHERTZ RADIATOR

BY

DOUGLAS G. BROWN

B.S. ELECTRICAL ENGINEERING
UNIVERSITY OF NEVADA, RENO

THESIS

Submitted in Partial Fulfillment of the
Requirements for the Degree of

Master of Science
Electrical Engineering

The University of New Mexico
Albuquerque, New Mexico

December 2010

Dedication

to

My daughter, who spent many nights with me studying late into the night,

or at least until bedtime.

Acknowledgments

First, I would like to thank my advisor Professor Christos Christodoulou for creating an opportunity for me to be able to work on this project.

I would also like to thank Professor Carl Baum for his tireless patience.

Most importantly I thank my wife, for her unending support.

OPTIMIZATION OF A TERAHERTZ RADIATOR

BY

DOUGLAS G. BROWN

ABSTRACT OF THESIS

Submitted in Partial Fulfillment of the
Requirements for the Degree of

Master of Science
Electrical Engineering

The University of New Mexico
Albuquerque, New Mexico

December 2010

Optimization of a Terahertz Radiator

by

Douglas G. Brown

B.S., Electrical Engineering, University of Nevada, Reno, 2004

M.S., Electrical Engineering, University of New Mexico, 2010

Abstract

At present, the utilization of the terahertz band for communications remains a hypothetical scenario. This thesis presents a design for a communications setup for terahertz frequencies of kilometer range distances using a reflector antenna design. The primary focus is the terahertz radiating element of the system. Building upon experimental work performed at the University of Oklahoma a simulation based approach is developed that duplicates experimental work. Next, this simulation setup is used with a new proposed design methodology is used to develop the primary radiators. A structure intended to be used with a photoconductive switch is selected and various design parameters are studied. The summation of the study concludes with a proposed experimental design that will be built and studied at the University of Oklahoma.

TABLE OF CONTENTS

List of Figures

List of Tables

Chapter 1

Introduction

One terahertz is one trillion cycles per second. Currently, the US frequency allocation only extends out to 275 GHz, or 0.275 THz [1] giving a clear indication of how ready this high frequency frontier is for development. The anticipated "Tera-Era" is expected to extend the limits of technology, promising higher bandwidths, faster communication, and more powerful processing capabilities. The benefits of pushing the upper boundaries of the frequency spectrum also extend beyond the immediate field of communications by offering more accurate spectroscopy, and less invasive medical examinations [2].

Currently the primary applications of the terahertz band are within the fields of imaging, security surveillance and spectroscopy, and sub-millimeter astronomy. Emerging applications of terahertz technologies are quite vast with publications in medicine, biology, space exploration, covert communications, compact radar ranges, industrial controls, terahertz microscopy, tomography, and various considerations for Homeland Security. There has been exponential growth in the field over the last four decades [3].

In this thesis, the primary focus is for communications therefore the topic of transmission through the atmosphere is of great interest. As such, atmospheric conditions

provide critical areas for concern in this frequency band. At the time of publication of this thesis, the furthest transmission in this bandwidth is 52 m at an operational frequency of 300 GHz, or 0.3 THz [4]. There are multiple reasons for the very short transmission distances that have been achieved in this bandwidth with the primary two being: the tremendous difficulty creating energy in this bandwidth, and the atmosphere itself may attenuate the energy at nearly 1000 dB per kilometer depending on frequency. Overcoming these obstacles creates a potential for this bandwidth to more readily used; not only by the fields that are already tapping its potential but also fields that require longer transmission distances such as communications and RADAR.

1.1   Terahertz Radiation

There is some variance in the general definition of the terahertz band. In this thesis the band of terahertz radiation is defined as 0.1 THz to 10 THz which is also consistent with other analysis [5].   This nestles in between the bands of microwaves and infrared energies. Figure 1.1 is a depiction of where in the electromagnetic spectrum the THz band falls.
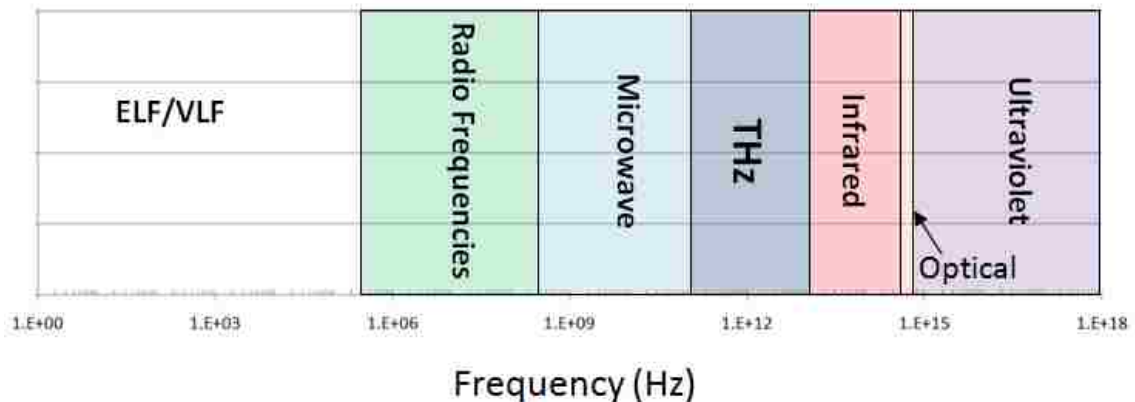
Figure 1.1. Terahertz Region of the Electromagnetic Spectrum

Immediately below the THz band lies the band of microwave energy which, has historically bundled the colossal fields of computer technologies, communications, and radar. The energy band above the THz band is infrared. In this bandwidth are technologies such as thermal scanners and cameras, and even infrared grills. Higher frequencies push into optical and laser technologies. In applying the electromagnetic spectrum the THz band has been frozen between these two gargantuan fields. However, the arrested development of the field has not been due to purely a lack of interest. In fact most experiments even today using the terahertz bandwidth show transmission across a laboratory in atmospheric conditions to be difficult [2], [4] [5] [6].

1.2   History of Terahertz Technology

This bandwidth is wedged between the well developed fields of microwave technology and optical technology. As such, researchers have used the techniques and hardware that have already being applied to one or both of these areas. They have attempted to blend the two fields in order to advance THz technology as THz lasers are not yet readily available and microwave sources do not extend into this frequency domain. This leaves a majority of laboratories exploring the THz field in generation and detection using a combination of physical planar and microstrip like structures to guide the radiation while the excitation for pulse generation and sampling is done with a laser. The recent explosion in terahertz technology can be attributed to the development of ultrafast short pulse laboratory lasers developed in the 1980's. Typical laser pulses to excite THz structures use a colliding-pulse passively mode-locked (CPM) ring dye lasers with pulse widths under 100 fs [5].

Techniques such as photo etching substrates and chemical vapor deposition are used to form these planar and microstrip like structures around a photoconductive switch. The sizes that the physical planar and microstrip structures that are studied are fabricated in a manner that is reflective of the wavelength that it is intended to be generated. The heart of this family of terahertz devices is the photoconductive switch. The switch is

3

grown from photoconductive materials that can take advantage of the capabilities of the recently developed ultrafast short pulse laboratory lasers. The first materials experimented with were a high resistivity silicon, or a Cr-doped Gallium Arsenide. Work that built upon these developments led to a Radiation-Damaged Silicon-on-Sapphire (RD-SOS). The advent of newer and better lasers allowed the progression of more advanced substrates. As of 2005 lasers are producing pulse widths less than 1 fs [5].

There are many available photoconductive materials available. However, the carrier lifetime of the material is extremely important in the application to the THz band. Table 1.1 shows common photoconductive materials that have been used in the THz field. Of critical interest to the frequency range of operation are the carrier lifetime and mobility of the material which are listed for reference [5].

Table 1.1- Characteristics of Ultrafast Photoconductive Materials [5]

Photoconductive Material	Carrier Lifetime [ps]	Mobility $\left[\frac{cm^2}{v \cdot s}\right]$	Resistivity [$\Omega \cdot$cm]	Band Gap (eV at R.T.)
Cr:doped SI-GaAs	50-100	$\approx$1000	10^7	1.43
LT-GaAs	0.3	150-200	10^6	1.43
SI-InP	50-100	$\approx$1000	10^7	1.34
Ion-Implanted InP	2-4	200	10^6	1.34
RD-SOS	0.6	30	-	1.10
Amorphous Si	0.8-20	1	10^7	1.10
MOCVD CdTe	0.5	180	-	1.49
LT-In$_{0.52}$Al$_{0.48}$As	0.4	5	-	1.45
Ion-Implanted Ge	0.6	100	-	0.66

R.T.: Room Temperature

A common photoconductor for various research groups is Low-Temperature grown Gallium Arsenide or LT-GaAs as it is used regularly in many different applications in the development of THz technology. LT-GaAs exhibits very short carrier lifetimes, on the order of 300 fs or less. These photoconductive properties were able to

be taken advantage of after the advent of Ti:sapphire sub-100 fs lasers as they exploit the extremely short carrier lifetime in GaAs that is less that 300 femtoseconds [5].

Detecting THz radiation has proven to be an endeavor comparable to the burden of its generation. As there are relatively very few generators of THz energy, there are a proportional number of detectors for the same bandwidth. Most THz radiating and detecting systems are built to be custom pairs of one another. That is the same device that can radiate THz is also capable of detection in the same bandwidth. Other options for THz detectors include Electro-optic crystals, interferometers, and optical methods of detection including bolometers [5].

The number applications of this technology is currently servicing are growing nearly every day. However, the majority of publications in the area are typically for uses in spectroscopy, imaging, and sub-millimeter wave astronomy [5].

Chapter 2

Motivation

Terahertz radiation is non-ionizing, penetrating to many opaque materials, scatters less than Near InfraRed (NIR) and diffracts less than all of the microwave band [5]. These are very appealing properties however, applications for THz in the field of communications are most commonly limited by their inability to be used at any appreciable distance [6]. This problem is not trivial as its solution requires ample generation of THz energy in such a way as to overcome atmospheric conditions as well as a strong highly directive antenna pattern that is capable of focusing the energy at a long distance.

In order to achieve greater transmission distances at the THz band, it is first important to generate enough energy at the band of interest to be capable of overcoming the associated atmospheric attenuation. This thesis proposes a Switched Oscillator (SwO) antenna design to achieve this goal. The SwO is a high-energy, pulsed-power photoconductive THz oscillator that in turn radiates at the intended frequency of operation. At the core of the device is a half wave microstrip resonator. The resonator itself is comprised of two oppositely charged plates that can be connected together electrically through the use of a photoconductive switch. The geometry of the SwO is shown in Figure 2.1.
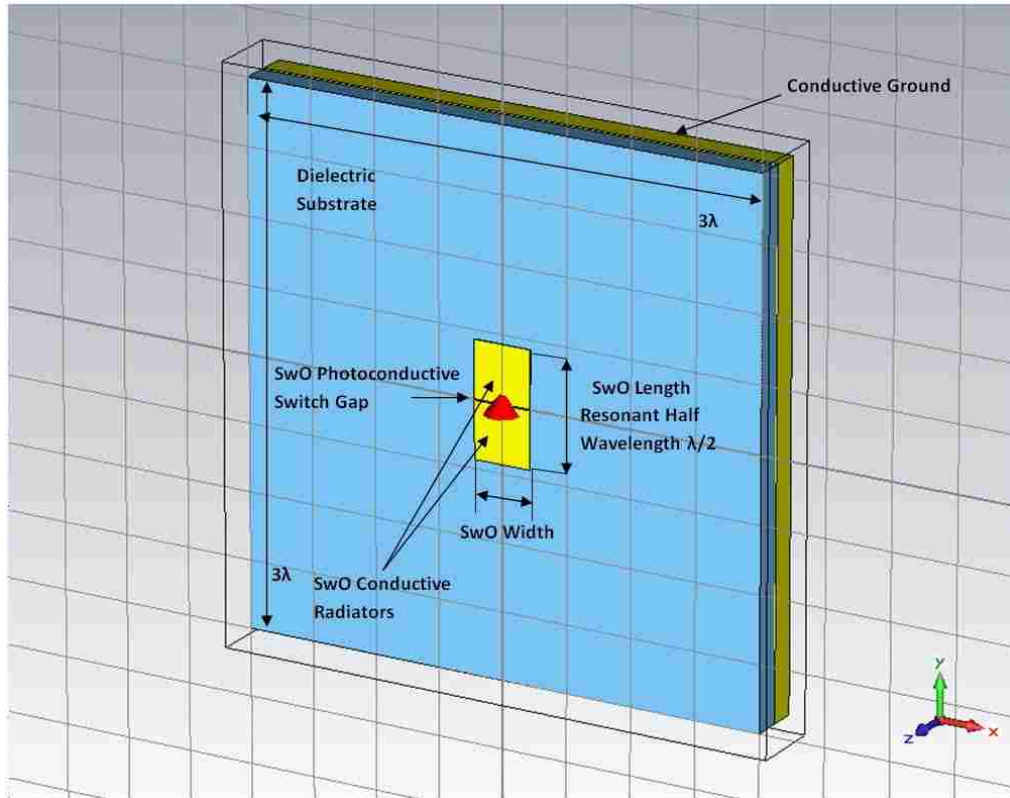
Figure 2.1. Physical structure of a SwO.

In effect the SwO forms a radiating half wave resonator in a microstrip transmission line. As photocurrents in the switch force an even potential between the two plates a wave front of current is generated through each of the rectangular elements. This wave front is then held within a self resonant structure that develops an effective half wavelength radiator based on the overall length of the SwO. Being resonant at the frequency of operation allows essentially all of the stored energy in the structure to be radiated at the desired frequency.

The design of the SwO is unique to other methods of generating THz energy in that the energy that is radiated from the system is stored within its radiating elements. That is to say the mechanism for energy storage is the designed radiators themselves. Other developments in the transmission and detection of THz use long coplanar transmission lines to both bias the antenna and isolate any secondary reflections from the

7

initial THz pulse. In contrast the SwO, being a resonant structure, is able to capitalize on the multiple reflections that are generated in its use.

2.1   Using Terahertz Technology for Communications

Many researchers are pushing the field of developing THz communications systems. Wireless data transfer rates have been increasing at exponential rates and are continuously pushing for more unoccupied bandwidth [6].

Generating frequencies with appreciable energy at higher and higher frequencies also becomes increasingly difficult as at higher frequencies discrete components must become smaller and smaller to account for the shorter wavelengths. The THz regime certainly does not deviate from this case.

Recent studies have shown drastic improvements in the transmission distances at a frequency of 0.3 THz. Initial studies showed transmission distances of up to 15 m and were later improved to a final distance of 53 m [5] [6]. Both cases were using a 0.3 THz system to transmit high definition video content.. A transmission distance of 53 m is far with respect to the distance of transmission for THz to date. However, this distance is much shorter than what simple hand held radios can achieve in lower frequencies. Increasing this transmission distance is a huge hurdle in applying THz technology.

2.2   The Role of the Switched Wave Oscillator

The SwO provides an elegant method for concentrating the radiated emission in the desired frequency of operation. The design of the device lends itself well to simulation studies by allowing a simulation domain to be designed so that the radiating parameters of the device may be carefully studied and optimized. However, a single SwO does not

in itself posses the entire solution to overcoming the challenges associated with transmitting THz over a significant distance.

The stored energy within a single SwO can indeed be maximized and its radiation characteristics optimized. However, an array of optimized SwOs possesses far better radiation characteristics than does a single device. In the far field of the device, the electric field increases proportional to the number of radiators in the array. However, the radiated power from the array is proportional to the square of the electric field resulting in the power radiated from the array being proportional to the square of the number of radiators. By utilizing this relationship of simulating and optimizing the radiation characteristics of a single SwO it will allow extrapolation to the number of SwO that are needed to bolster the electric field to the level necessary to overcome atmospheric attenuation. Thus an array of many SwOs can be designed to achieve the required field strength.

2.3   Approach for Using the Switched Oscillator

Clearly, the design of the radiating THz system begins with the design and optimization of the SwO. However, there are many other designs that have been employed in the THz regime.

The rectangular plate design has been adopted as it is resonant at a specific frequency. Being resonant at a single frequency allows the spectral content of emission to be focused at the resonant frequency. Thus, the Power Spectral Density (PSD) is as concentrated as possible at the frequency of transmission. This approach has obvious advantages when one considers the hurdle of overcoming atmospheric attenuation.

A bowtie antenna design has been explored in [5]. The inherent nature of the bowtie is a broadband structure as the tapered sides of the antenna harbor a plethora of longer and shorter wavelengths proportional to the arc in the bowtie. With the bowtie radiating its stored energy over a wider bandwidth than that of the SwO the PSD of any

frequency will be lower than that of the SwO. In the far field of the antenna, a lower PSD directly translates into a shorter distance that the device may transmit and overcome atmospheric attenuation. This gives the SwO a clear advantage over a bowtie approach as its narrow band resonance focuses the majority of its radiation into the transmission frequency. It is for this reason that wide band antenna designs have been abandoned in this thesis as they all will radiate a lower PSD that will have greater difficulty overcoming atmospheric attenuation. A generic schematic of a bowtie antenna is shown in Figure 2.2.
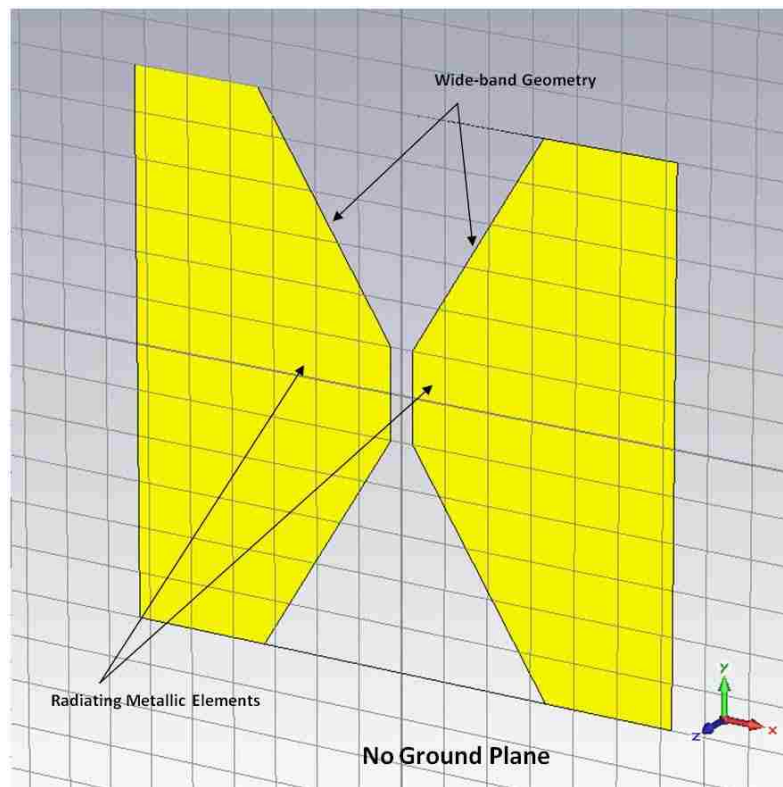
Figure 2.2. Bowtie antenna schematic.

Other approaches to overcome the difficulties of transmitting at THz have been to build the radiator on the photoconductive switch such that the triggering laser approaches from the side of the antenna. This design allows that the transmitted energy from the antenna is now traveling through the substrate to the detector. In the SwO, the ground plane allows the two planar radiators to store more energy as each radiator forms a

parallel plate capacitor. This effectively stores the energy that will be radiated by the SwO in the dielectric that separates the radiating plates from the ground plane. The SwO has another clear advantage in the application of transmitting energy over a design without a ground plane as the SwO radiates into the space that is only above the antenna. As such, the SwO only radiates in the direction of the intended target and eliminating the unused half space behind the antenna; this immediately doubles the transmitted energy. Finally, the SwO transmits through air and not a dielectric medium allowing minimal impedance reflections in transitioning from media to the next.

The most common photoconductive THz antenna design is a planar dipole that is contained within two long coplanar transmission lines. This design is chosen for its relatively narrow spectral output and its short THz pulse. While the coplanar transmission lines offer an immediate method for biasing the antenna, the intent is to segregate the initial THz pulse from any secondary reflections that occur from the unavoidable impedance mismatch from the closing switch. In isolating the initial THz pulse from secondary reflections only a portion of the stored energy within the radiating structure is able to be radiated. In contrast with the SwO, it is designed to radiate the vast majority of the stored energy within the structure.

Lastly, initial considerations for the SwO were to use the device to feed a THz antenna structure. In this case the SwO is used as a THz current source that then feeds a tuned THz antenna. For this design, each length of the zigzag, or serpentine in the SwO is kept at a length of a half wavelength, or the overall length of the SwO. As such, the currents in each length of the antenna collectively add to the overall radiation from the antenna. The relative width of the THz antenna is kept relatively narrow with respect to the SwO as this creates an impedance mismatch between the SwO and the antenna. The antenna having a higher impedance than the SwO can nearly double the exciting voltage at the base of the antenna [8] [9]. Schematics that use a SwO fed antenna are shown in Figure 2.3.
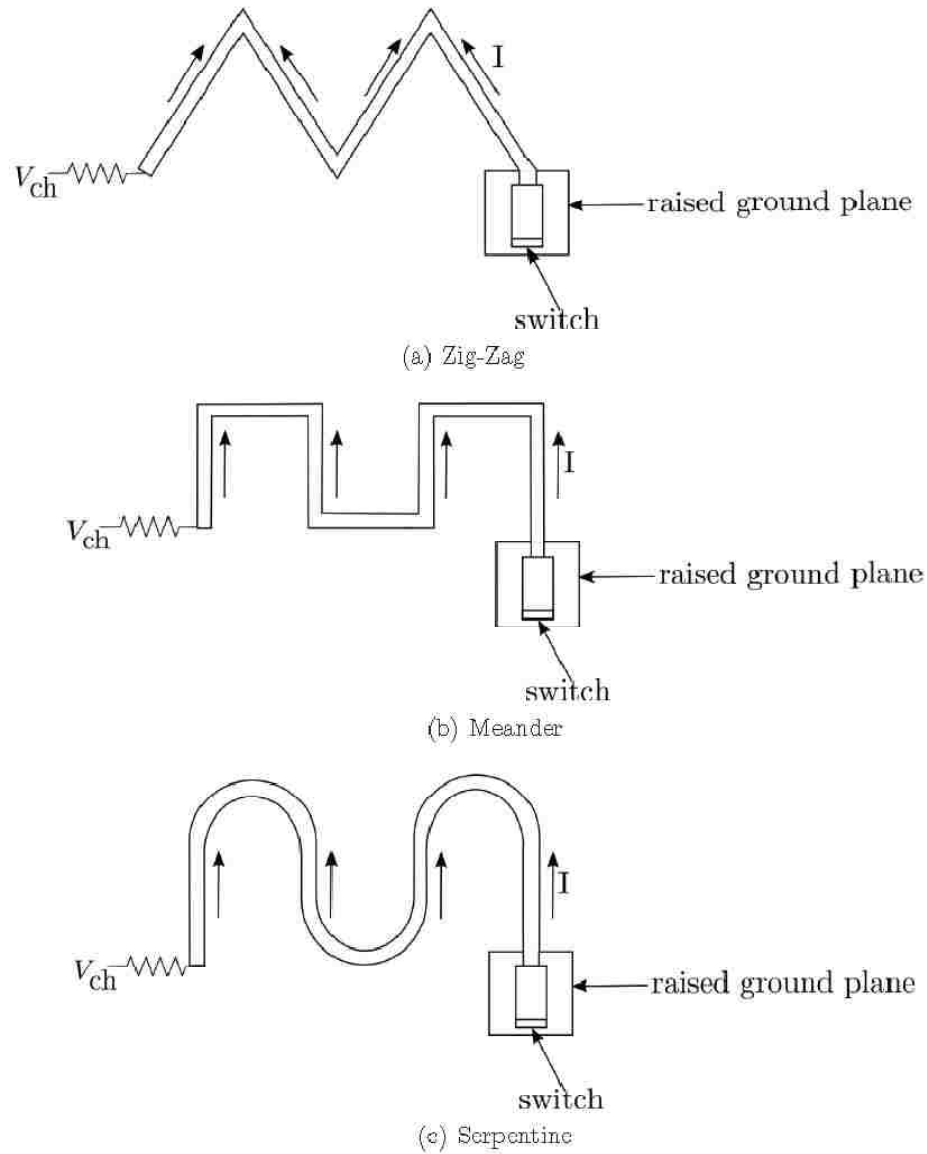
Figure 2.3. Zig-zag and meander antennas driven by a SwO [8].

This general form for using the SwO to couple THz energy to a THz antenna was abandoned as research has indicated that the SwO is an effective radiator as it forms a Hertzian dipole mounted above a ground plane. Using only a SwO significantly reduces the complexity of the overall design and creates a more simple simulation space that is required for optimization.

It is for these reasons that the approach of this thesis is to fundamentally simulate and optimize each parameter for the SwO. A centralized focus on this THz radiator is chosen over a comparison in simulation of other THz antennas as the SwO has not been developed as a THz antenna. The SwO represents a unique approach to a THz radiator. Focusing on its design allows that this concept be developed as thoroughly as possible so that it may be experimentally tested and compared with simulated results.

Chapter 3

Terahertz Antenna Simulation

Developing an accurate simulation setup is critical in developing the SwO. In order to accomplish this, a simulation setup of an existing Terahertz experiment performed at Oklahoma State Universities' Ultrafast Terahertz-Optoelectronic Laboratory (UTOL) will be performed. This will show that the simulation setup in CST is accurate for the development for the SwO. The effort will work as a proof of principle in laying the baseline for simulation studies.

The design approach will be to use the time domain solver within CST to calibrate numerical results to analytically derived results from [8]. For the setup within CST there are many factors that require attention to ensure that the simulation domain is as accurate as possible.

There are general rules that must be observed when using CST [9]. When using an FIT solver the Lines-Per-Wavelength (LPW) represent how the simulation space is broken into discrete spaces for simulation. The simulation needs to be meshed with a minimum of 10 LPW throughout the simulation domain. This is to ensure that there is an even transition in the electric and magnetic fields in the simulation space to make the representation of the fields as accurate as possible. This also minimizes numerical instabilities throughout the simulation domain. The number of LPW is directly

dependent upon the excitation for the simulation. It is also important to pay close attention to electrically small features in a simulation as, though the overall simulation domain may be meshed appropriately, meshing around any electrically small feature may not be. These are primary rules. Due to the unique characteristics of each design every simulation will require different considerations and each will have specific nuances that need to be addressed in the design and execution of the simulation.

3.1   Experimental Work at Oklahoma State University

The work that will be compared to from UTOL specifically uses Professor Daniel Grischkowsky's published data on terahertz technology. For the application described Grischkowsky's physical setup of a 5-10-5 Max1 Antenna will be used for comparison. The approach for this problem is thus now from both simulation and experimental directions. For the purpose of this study the physical setup described below will be used for calibration of the simulation approach. It has already been fabricated and tested at UTOL and therefore provides a known response.

The "5-10-5 MAX1" antenna is constructed of 0.5 µm thick aluminum radiators and coplanar waveguides atop a 0.5 µm thick layer of ion implanted silicon. This is formed on a 200 µm layer of sapphire forming the antenna substrate, this configuration is shown in Fig. 3.1.
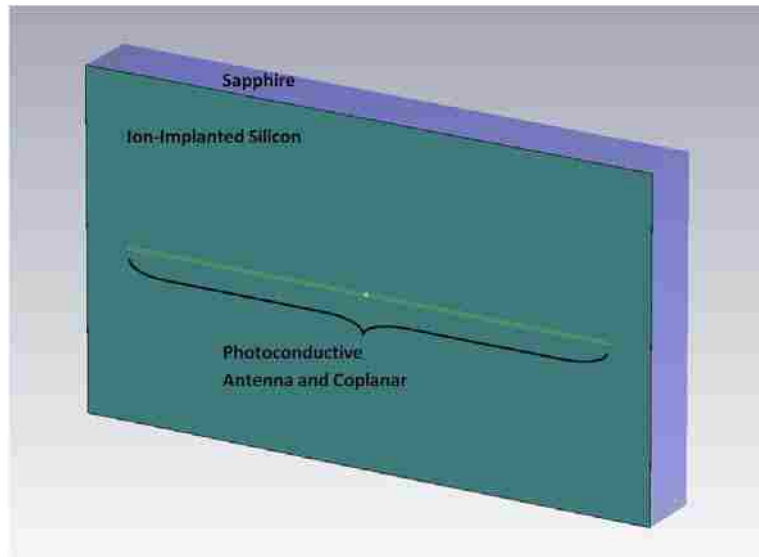
Figure 3.1. 5-10-5 MAX1 antenna at UTOL [10].

At the center is a Hertzian dipole with two rectangular radiators that are constructed into the coplanar transmission lines. The Hertzian dipole elements themselves are 10 µm wide by 7.5 µm long separated by a 5 µm gap. The overall length of the radiation structure is 2 cm, resulting in coplanar waveguides in either direction that are 5 µm wide and 1 cm long spreading from the center dipole [8].
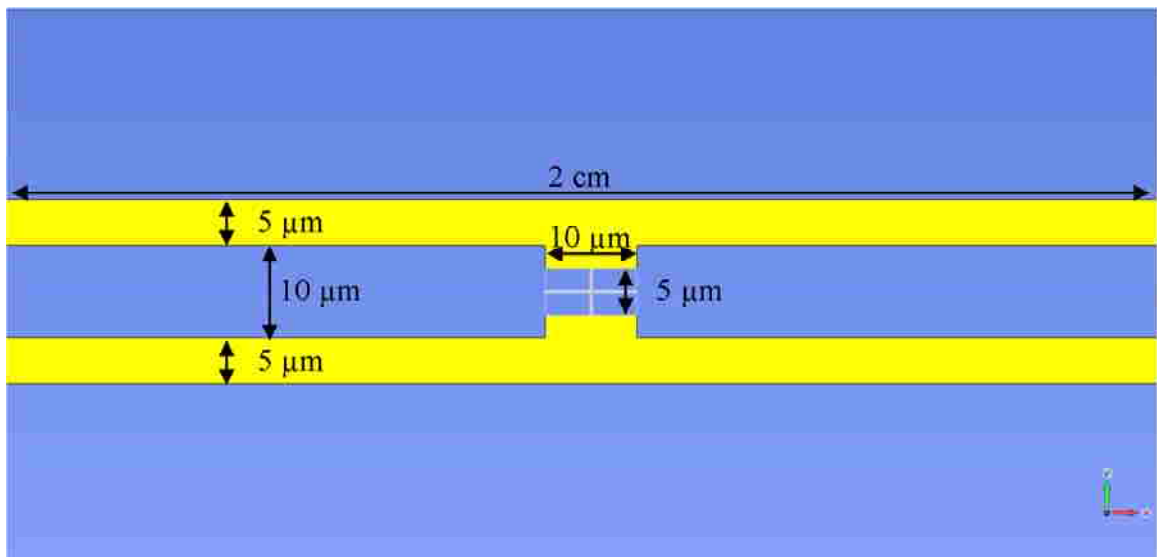
Figure 3.2. 5-10-5 MAX1 antenna at UTOL zoom [10].

The length of the coplanar waveguides is designed such that, as the radiating Hertzian dipole is initially triggered, an impedance mismatch forces a reflected wave down the coplanar waveguide away from the dipole. This wave travels the length of the transmission line before it is reflected a second time back towards the antenna. The length of these coplanar transmission lines is made long enough to ensure the reflected signal does not interfere with the initial radiated pulse from the antenna [10].

The Hertzian dipole antenna and the two long coplanar transmission lines are formed using a chemical vapor deposition process. After fabrication the coplanar transmission lines are biased at a voltage of up to 60 Volts. A femtosecond class laser is used as the excitation source for the antenna as it is focused on the photoconductive switch gap. The laser that is used is a Colliding-Pulse Mode-Locked dye laser that focuses 5 mW of 623 nm photons in an 60 fs excitation pulse [10]. As the laser is fired a conducting path at the center of the dipole is formed allowing currents to flow through the switched area of the antenna.

The emitted THz radiation is then collected by a silicon lens that is attached to the Sapphire substrate that focuses the radiated energy toward a series pair of paraboloidal mirrors towards a second identical 5-10-5 THz antenna that acts as a receiver for the transmitted energy [10]. A depiction of the laboratory setup is shown below in Figure 3.3.
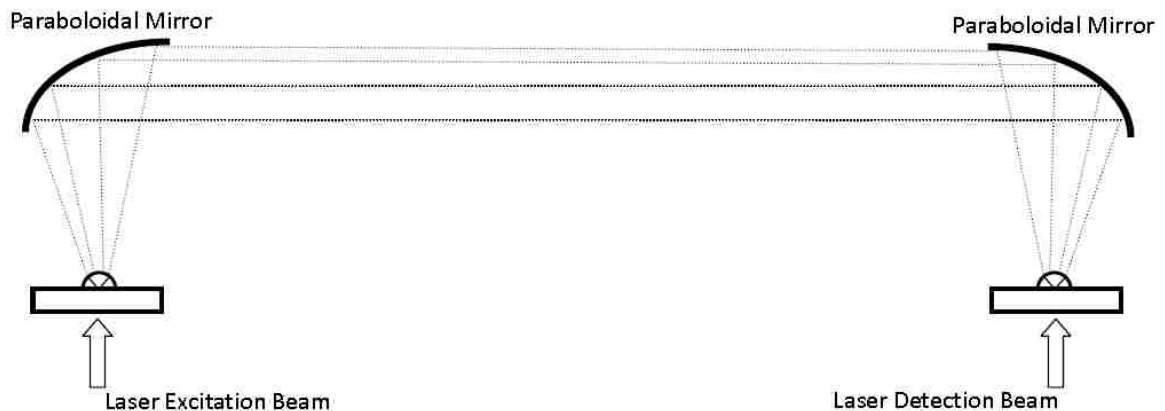
Figure 3.3. UTOL laboratory setup [10].

The physical distance between the antennas and the paraboloidal mirrors is 26 cm. It is reported that due to the exceptionally low dispersion and absorption of silicon the 13.5 mm propagation through the silicon lenses do not significantly affect the radiated pulse shape of the radiated THz pulse [10].

3.1.1 Terahertz Antenna Excitation

Using a photoconductive switch as the excitation mechanism for the THz structure does not allow a direct method in determining the current profile that excites the structure. Instead, one has to use secondary methods to measure the exciting current. The first unknown characteristic of the profile being the rise time of the laser that is focused on the switch, and the second being the carrier lifetime of the photoconductive switch.

UTOL has measured the optical pulse that is used in conjunction with the photoconductive switch as a Gaussian shaped pulse with a FWHM of 60 fs [10]. The ion implanted SOS has a carrier lifetime reaching a fast limit at 600 fs with longer carrier lifetimes achieved at lower doses of ion implantation [11].

In order to experimentally determine the waveform of the exciting current, the change in reflectivity of the photo conducting switch may be measured [11]. The results of which are shown below in Figure 3.4.
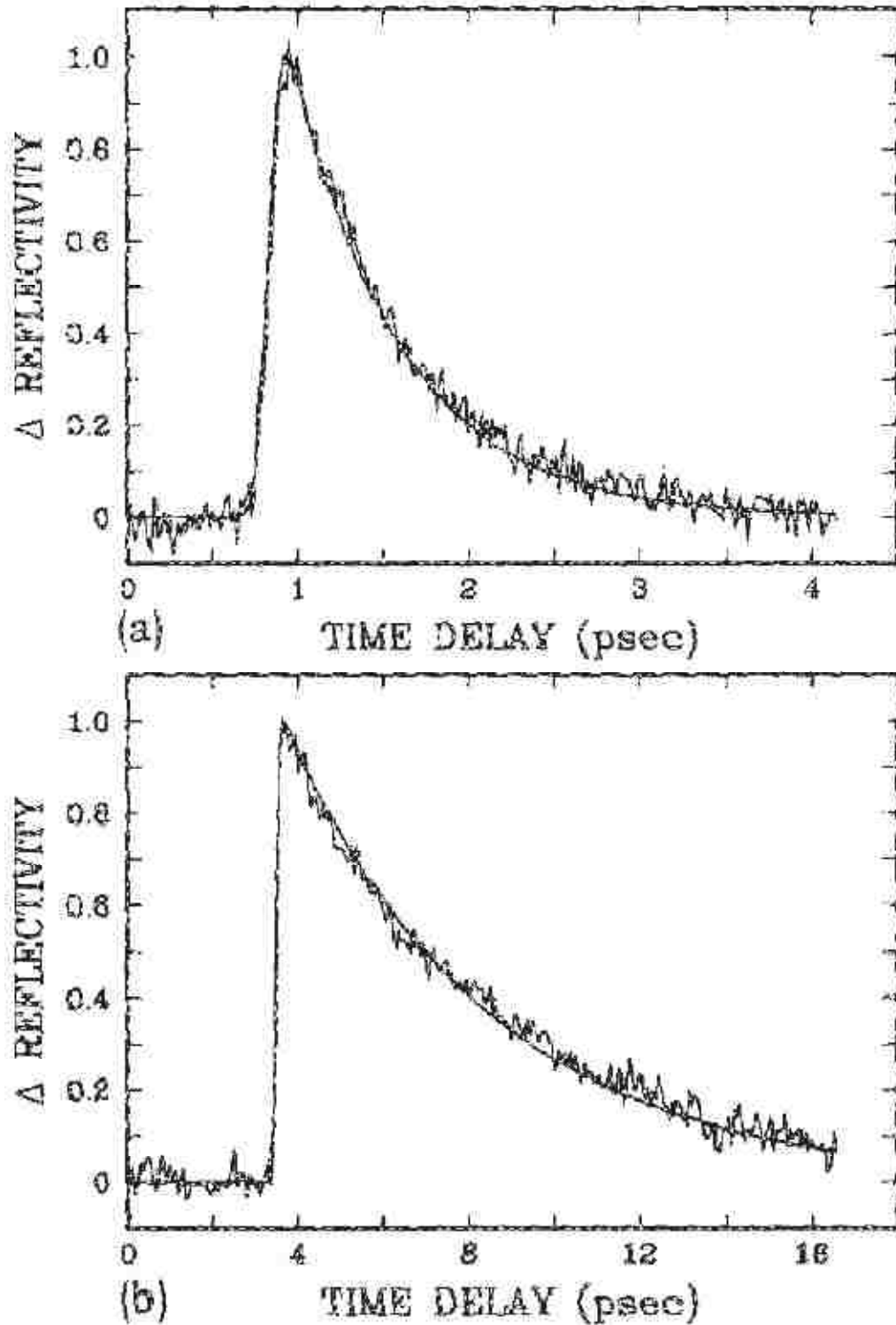
Figure 3.4. Measured change in reflectivity for SOS samples ion implanted at doses of (a) 2 x 1015 cm-2 and (b) 1 x 1013 cm-2 [11].

Using the physically measured properties of reflection, a basic Drude model is adopted such that the mobility of electrons and holes as well as their associated lifetimes are taken into account inside the photoconductive switch [10]. The Drude model itself is a relatively simplistic model that is used to understand electrical conduction [12]. Here it is used to describe the characteristics of a dielectric where it treats the free carriers in the solid as classical point charges that are subject to random collisions [13]. The Drude model can be applied so that the relative permittivity of the dielectric can be expressed as:

$$k = k' - jk''$$

Where k', and k'' are developed to be functions of resistivity [13]. Thus, through time, the voltage across the gap is known and the time varying resistance is also known yielding a current profile across the gap. This provides an indirect method for measuring the current through the gap that is proportional to the measure of reflectivity of the switch.

3.1.2 Terahertz Antenna Radiation

The radiated THz pulse in the small antenna limit is shown to be the derivative of the input excitation current [10], [11]. [12]. Experiments at UTOL have corroborated these results showing that for different sized antenna elements the radiated THz pulse is dependent upon the rise time of the laser excitation and not the physical size of the Hertzian dipole antenna [10]. It was determined that the analytically derived waveform for the radiated THz pulse matches the measured THz pulse [10]. The current pulse and its associated time derivative waveforms are shown in Figure 3.5 (a) and (b). The associated spectral content of the analytically anticipated radiated pulse is then shown in Figure 3.5 (c) and then it is overlaid with the measured spectral content in Figure 3.5 (d).
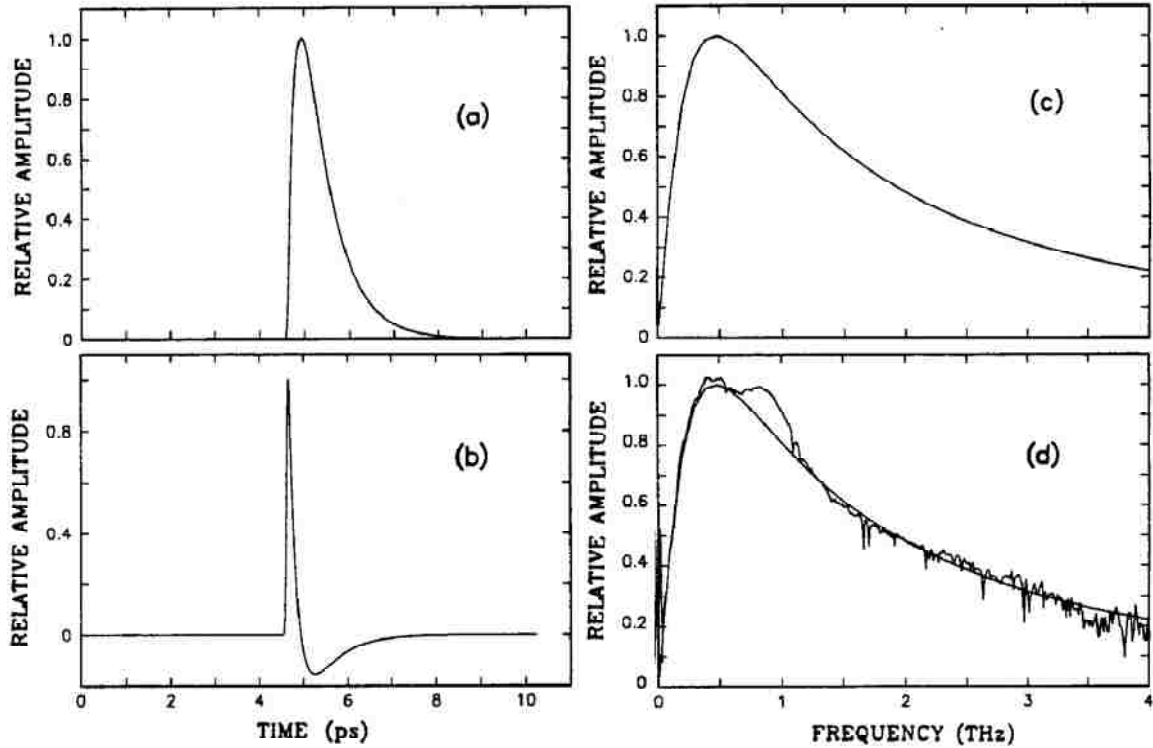
Figure 3.5. (a) The calculated current pulse in the antenna (b) The time derivative of the current pulse (c) Analytical spectral amplitude (d) Comparison between the analytical result and the experimental result [11].

The results show excellent agreement and will later form the basis for proving that the simulation setup in CST is accurate.

3.2   Reproducing Experimental Results Through Simulation

The first step in setting up a simulation to validate the approach described in section 3.1 is to virtually build the physical geometry. However it becomes immediately evident that building coplanar transmission lines in CST of the required length will make the simulation domain too large to be capable of simulation. To overcome this problem one must return to the first principles of the design. It is known that the intent of the length of the coplanar transmission lines is to inhibit reflection from the initial excitation of the

21

dipole from impending upon the initial radiation pulse. Thus a shorter coplanar transmission line may be used as long as this characteristic of the assembly is preserved. And it is, in fact, possible to accomplish this feat with shorter coplanar transmission lines. In setting up the simulation domain, it is found that the length of the coplanar transmission lines is adequate at an overall length of 3.0 mm.

The physical geometry that was used for simulation in CST is shown in Figure 3.6
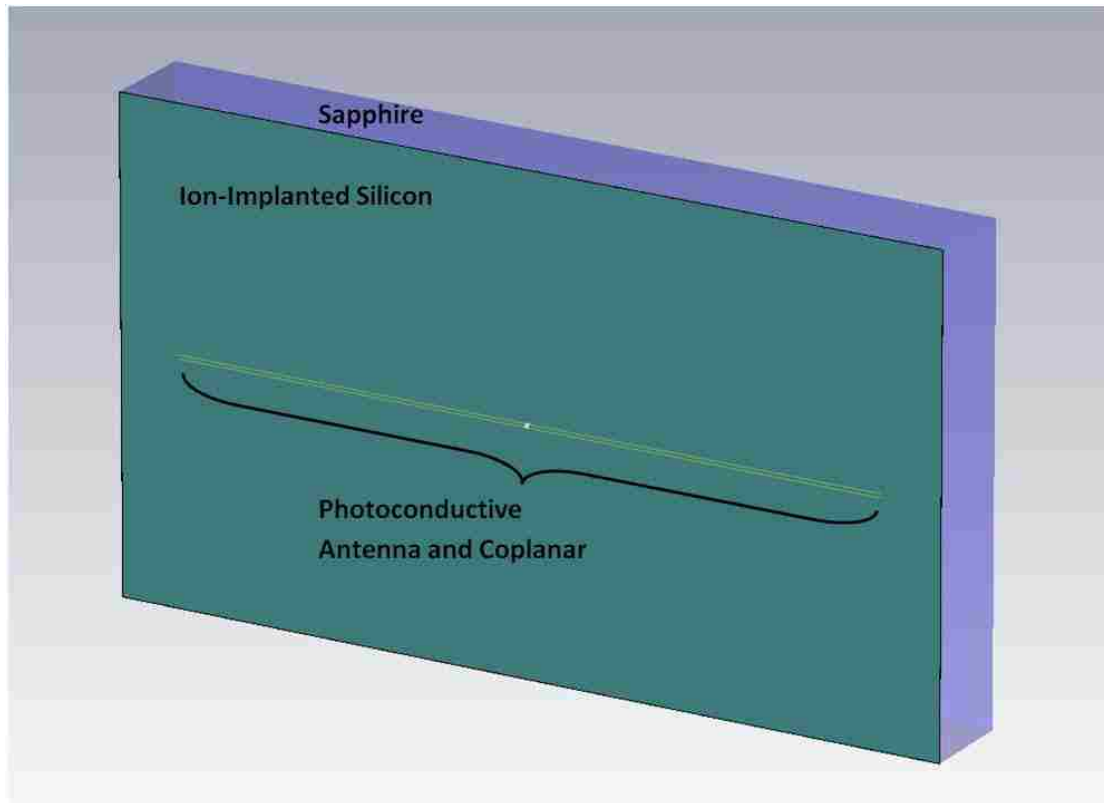
Figure 3.6. CST Simulation of a MAX 5-10-5 Antenna.

A closer depiction of the Hertzian dipole at the center of the antenna is shown in Figure 3.7.
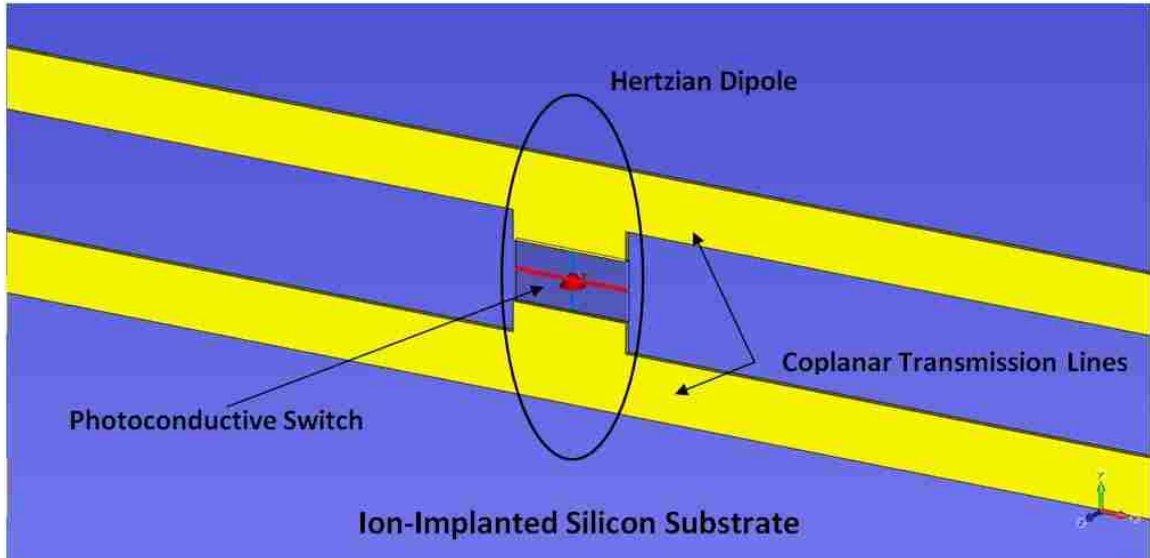
Figure 3.7. CST Simulation of a MAX 5-10-5 Antenna: Close up of Hertzian Dipole.

The physical dimensions of the simulation for the Hertzian dipole portion of the simulation setup mirror that of the given 5-10-5 MAX1 antenna.

The photoconductive switch is modeled in two steps. The first is as a face port that connects the two elements of the antenna together. The second is an approach to model the excitation that mirrors as closely as possible the current pulse used in the original test setup of [10].

3.2.1 The Reciprocal of the Sum of Two Exponentials Excitation

The meshing requirement within CST for a minimum of ten lines per wavelength at the highest frequency of excitation. As has been reported the FWHM of the laser excitation pulse is 60 fs [11]. The rise time of the pulse determines the maximum frequency that is seen in the spectral domain. A Gaussian pulse with a FWHM of 60 fs has spectral content out to 16 THz. This yields a condition that is not capable of being simulated within CST under current reasonable computation capabilities.

23

In order to proceed, a pulse shape that mimics the excitation current as closely as possible must be derived [7]. This new pulse shape, defined as the reciprocal of the sum of two exponentials excitation [8], is designed to give a t_{mr} of 0.5 picoseconds. The comparison of the two exciting currents in Figure 3.8 shows that they are indeed very close.
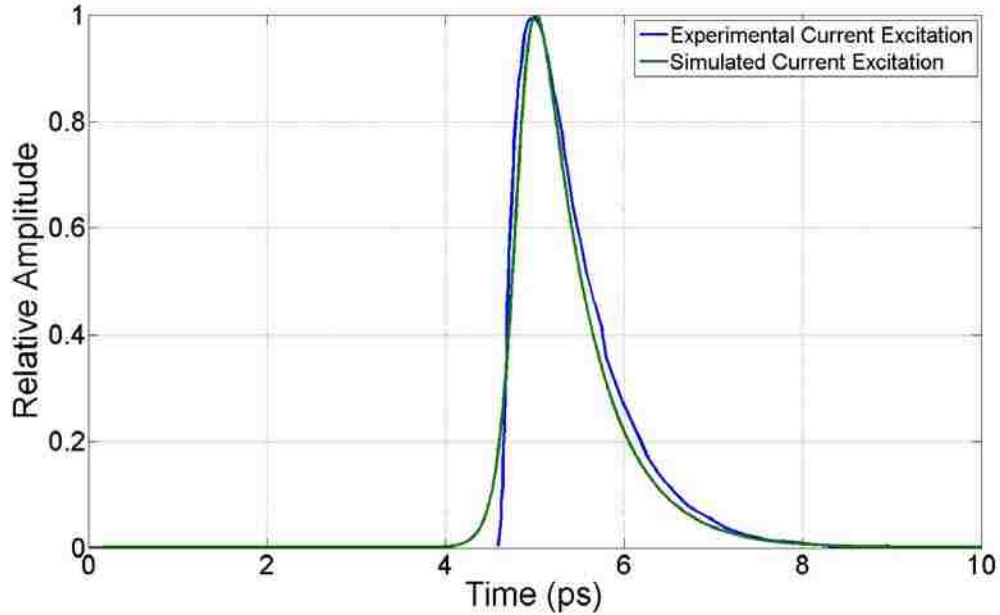
Figure 3.8. Comparing the Published Data for the Current Excitation to the RSEE Pulse

A graphical comparison of the two excitations is given in Figure 3.8. The spectral content of the excitation is shown in Figure 3.9.

24
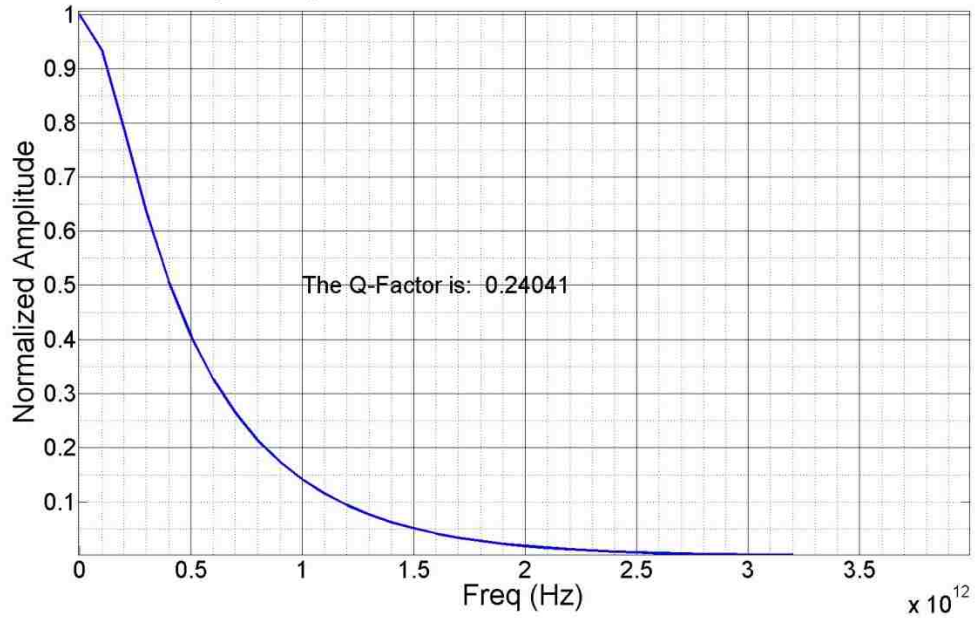
Figure 3.9. Spectral Content of RSEE Excitation Pulse.

This excitation does allow meshing at a much lower rate, nearly 3 THz instead of 16 THz.

It is anticipated that the result will be what has been previously demonstrated in [10], [11]. That is the anticipated radiated waveform is the time derivative of the input current pulse. Presuming this is true the time derivative is shown Figure 3.10.
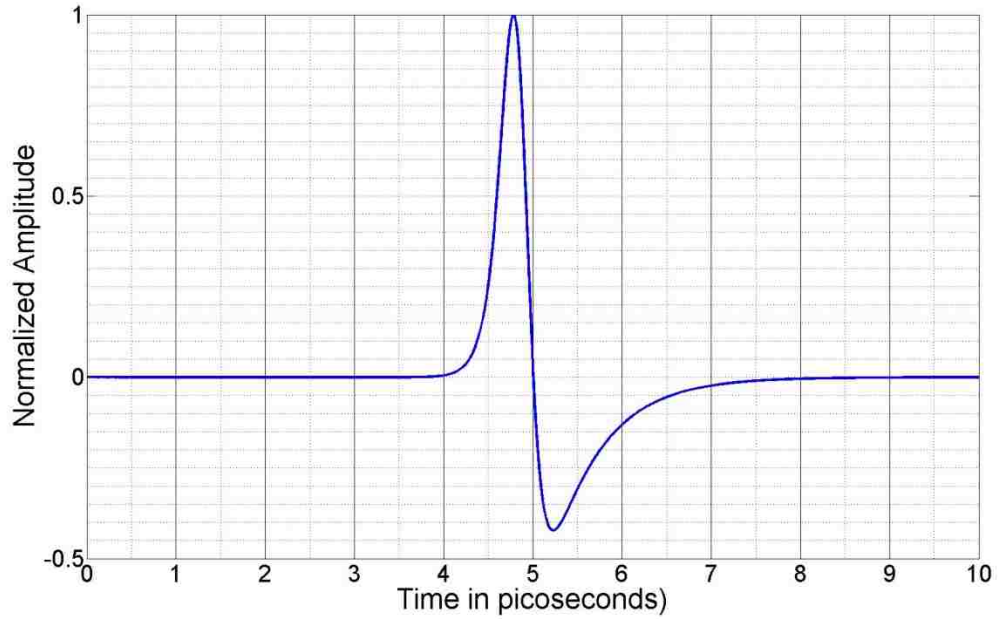
Figure 3.10. Time Derivative of the RSEE Excitation Current.

The radiated THz pulse along with its anticipated spectral content will be used as the bench mark for measuring the results of the CST simulation for their accuracy. The anticipated spectral content is shown Figure 3.11.

The Q-Factor is: 0.74041
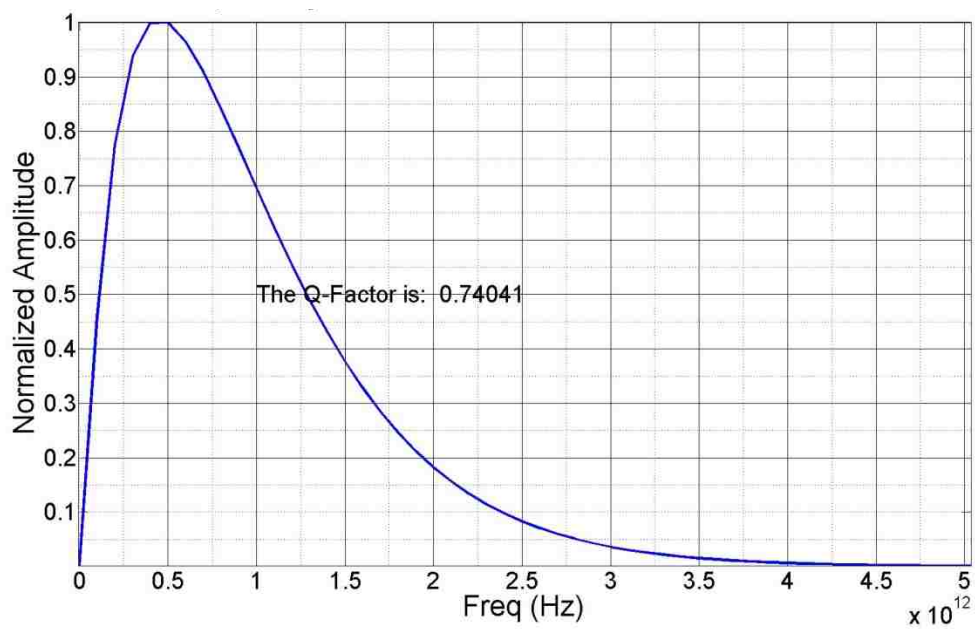
Figure 3.11. Spectral Content of the Time Derivative of the RSEE Pulse.

26

3.2.2 Simulated Results

The time domain radiated pulse from the experiment is shown Figure 3.12.
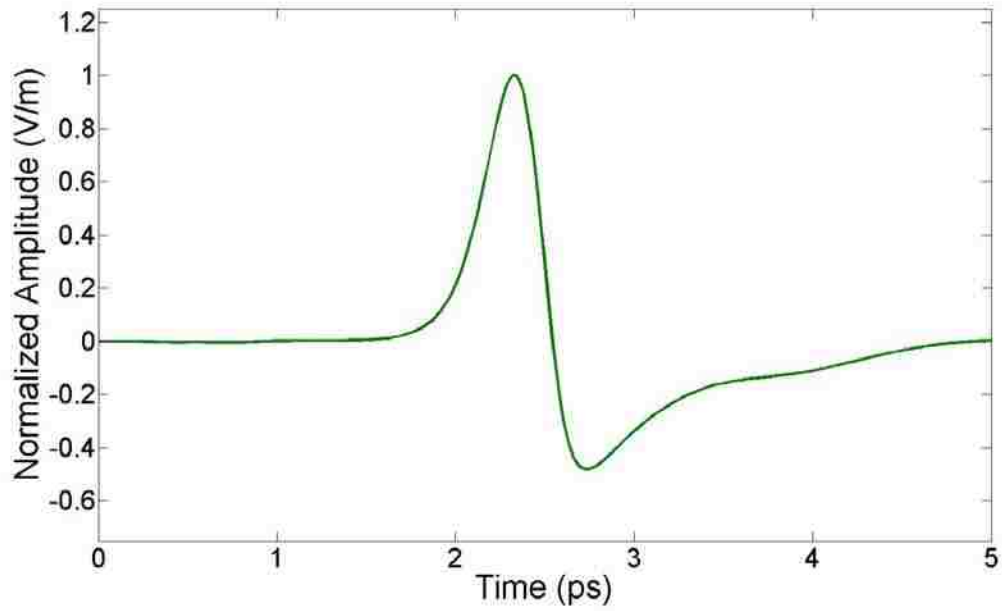
Figure 3.12. Simulated 5-10-5 Max1 antenna output.

By overlaying the analytical result on top of the simulated result in Figure 3.13 shows that the simulation is in excellent agreement.
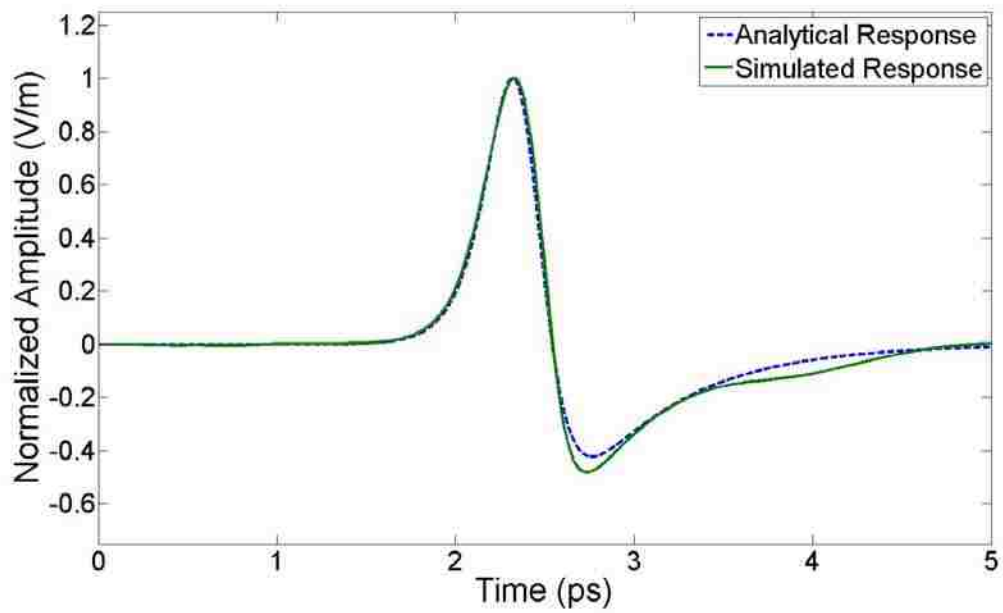
3.13. Analytical vs. simulated results.

Lastly, the spectral responses of the analytical result are overlaid with the spectral response of the simulation Figure 3.14.
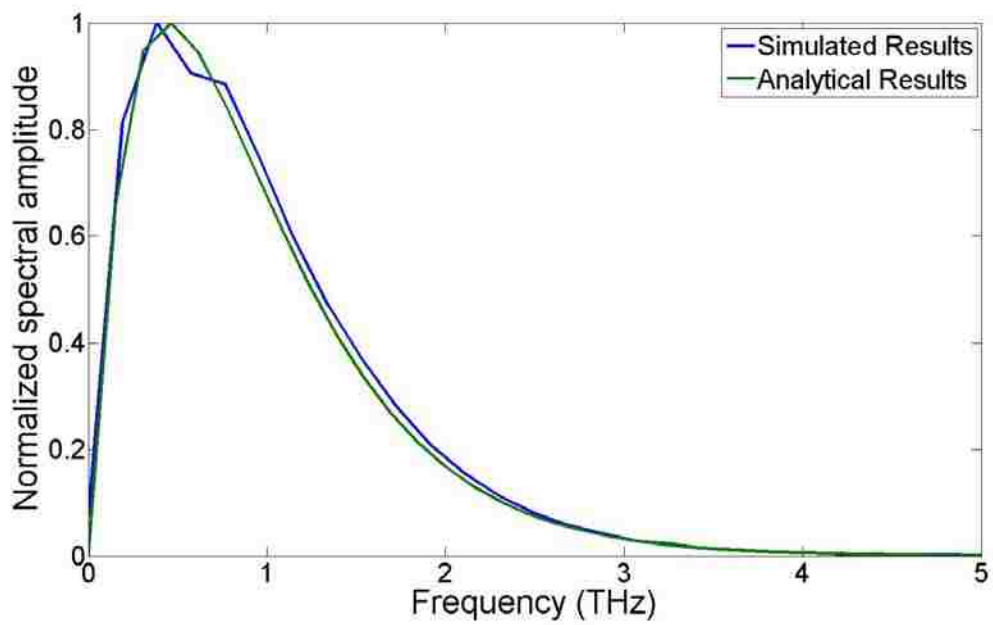
3.14. Simulated vs. analytical spectral responses.

All comparisons of simulated results to analytical results show very close responses in the temporal and spectral domains. There are slight differences in the later time for the temporal response and that difference is reflected in the spectral domain. However, these slight differences do not detract from the very good reproduction of data. As such, these results show that the simulation approach is valid.

3.3   Conclusion of Simulation Study

The work done by UTOL does lead to a very straightforward method for testing the simulation domain. Experimental parameters have been provided for the physical setup, and both temporal and spectral results compare very well with theoretical results.

The net result shows that the FIT solver in CST is capable of producing reliable results as it has successfully reproduced the experimental results in the work at UTOL. The intricacies for the reproducing the results do require that the physical setup is accurately reconstructed, and the excitation be understood and modeled accordingly. As this is the case for the SwO one can assume that accurate results will be produced in the study of the SwO. It is this that allows not only CST, but this modeling approach, to be used in the development of the SwO.

Chapter 4

The Switched Oscillator

In comparison to the THz radiators that are developed at UTOL, the switched wave oscillator is designed to be a self resonant structure. Whereas the antennas at UTOL are designed with long coplanar transmission lines to divert secondary reflections from entering into the intended THz pulse, the SwO utilizes these reflections to bolster its total radiated power. For the SwO those reflections are controlled in their spectral content through the geometry of the SwO by design. By controlling the spectral content of the oscillations and pushing them back into the radiating area of the antenna the majority of the stored energy in the structure may be broadcast into a THz chirp.

4.1   Introduction to the Switched Wave Oscillator

A single SwO is itself a pair of oppositely charged square patch antennas separated from each other by a photoconductive switch. The pair of square patch antennas is then separated from a ground plane by a dielectric. Each dimension is rigorously designed to

ensure optimum radiation characteristics are obtained. Shown in Figure 4.1 is an example of the SwO.
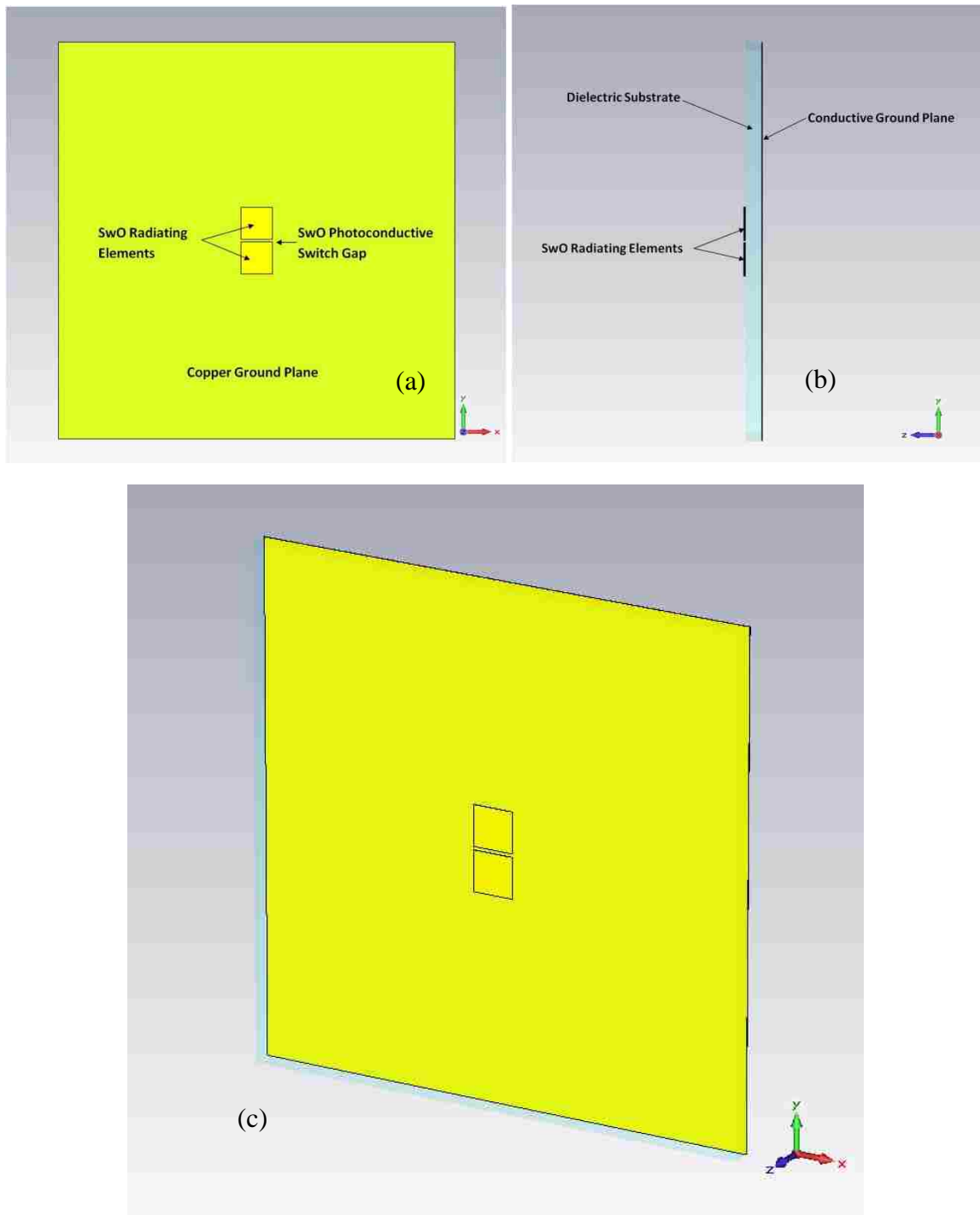
Figure 4.1. (a) front view of the SwO looking down onto the square patches and photoconductive switch (b) side view of the SwO with the dielectric that spaces the radiators from a ground plane (c) overall perspective of the SwO.

The output of the SwO is a pulsed damped sinusoidal waveform that is related to the frequency by the overall physical dimensions of the radiator. For the purpose of clarity Figure 4.2 shows a schematic view of the SwO and defines the physical geometries to which the SwO is constructed.

(a) Side view
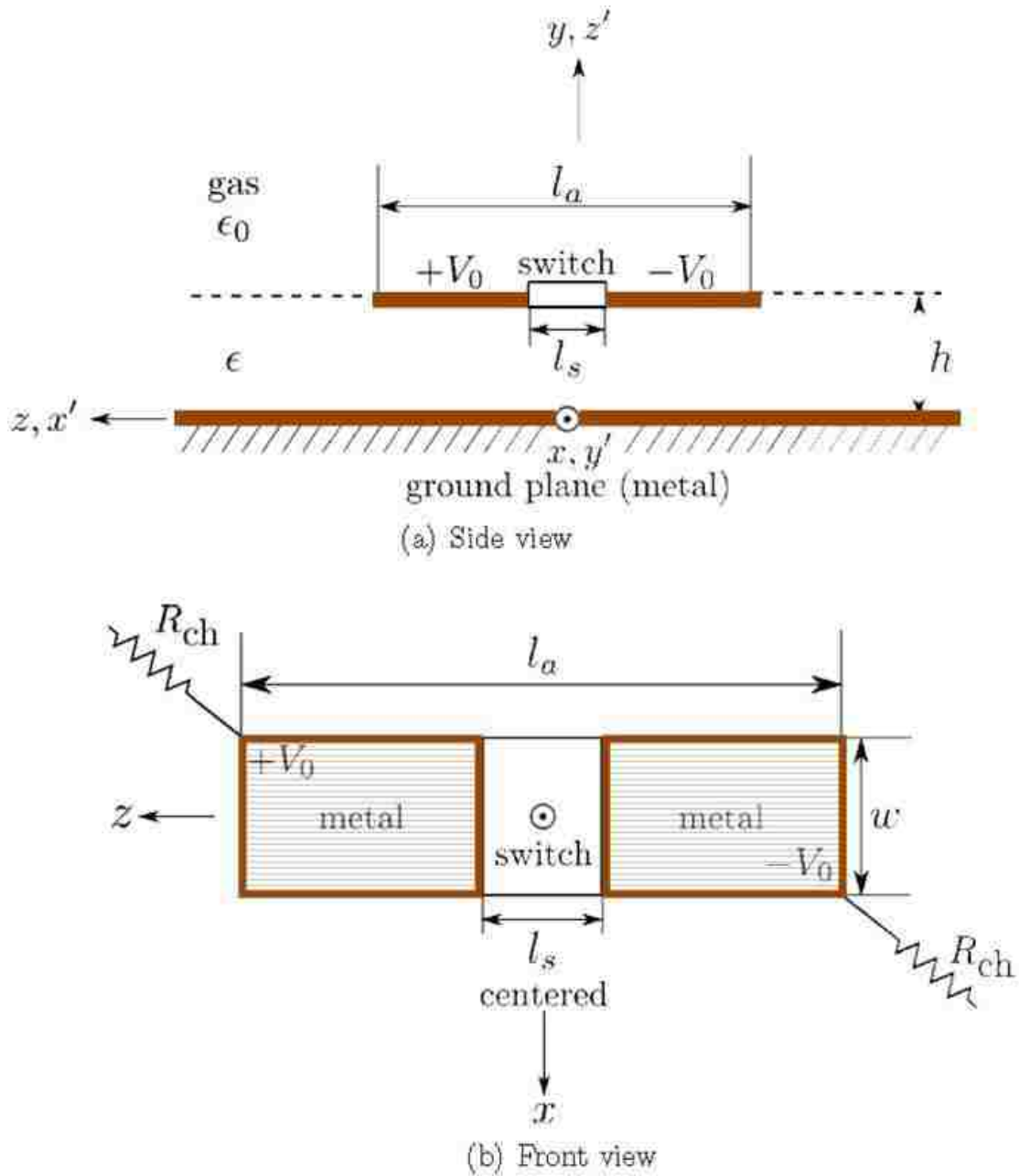
(b) Front view

Figure 4.2. SwO Schematic (a) Side View (b) Front View [14].

As illustrated in Figure 4.2 the metal ground plane sits below the radiator at a distance h. The overall length of the radiator is designed to be a half wavelength long and is denoted by l_a. The length of the switch is l_s. The width of the radiator is shown as w and lastly, the dielectric has a permittivity of ε.

These various physical parameters make up the design space for optimizing and simulating the SwO. As such each will be independently varied to show functionality and overall system performance impacts. For comparison purposes, quantities of Quality factor, center frequency, peak radiated electric field, and radiation gain will be analyzed.

4.2   The Switched Wave Oscillator as an Antenna

In essence, the SwO forms a planar center-fed dipole antenna with the two rectangular radiating elements acting as separate arms of the dipole. The photoconductive switch is used to isolate the two rectangular radiating elements of the SwO as they are charged to equal and opposite voltages. A high speed material such as those listed in Table 1.1 must be chosen for the switch. This ensures that the switch is compatible with the THz spectral content. A femtosecond class laser is then used to focus energy onto the photoconductive switch. The laser pulse shorts out the potential difference that is stored within the SwO resulting in the exciting photocurrents on the SwO.

The input excitation for the SwO is defined as a voltage step input representing the charged voltage potential, from the biasing lines, across the gap before the laser pulse with there being no voltage potential during and immediately after the laser excitation [14]. Prior to the laser pulse there a potential difference between the two rectangular radiating elements of the SwO exists, and after the laser pulse the two elements are brought to a potential equilibrium.

A true step input or a ramp rising step provide a condition that cannot be simulated as they contain frequency components that are very high and lead to mesh sizes that cannot be reasonably simulated. Thus a smooth voltage step input to the SwO is used as it most closely represents the previously derived conditions [14]. An example of this smooth step is defined by its total t_{mr} rise time and is shown in Figure 4.3.
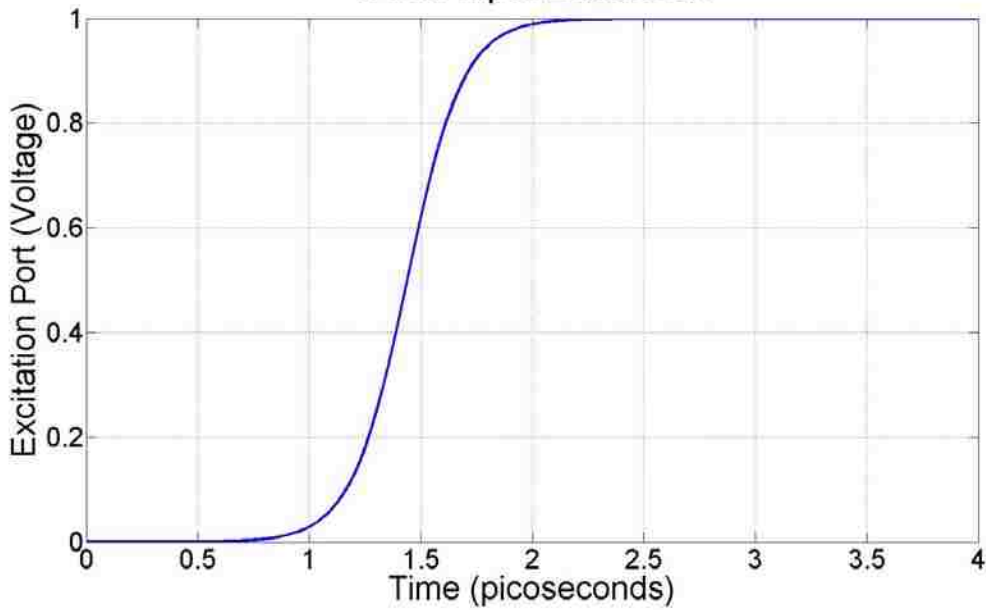
Figure 4.3. SwO input excitation as defined by T_{mr}.

The definition of t_{mr} is that of the time of max rise. It is defined for a pulse such that the maximum, is then divided by the maximum time derivative. It is shown in equation form as follows **Error! Reference source not found.**.

$$t_{mr} = \left[\frac{d}{dt}f(t)\Big|_{max}\right]^{-1} = E_{max}\left[\frac{d}{dt}E(t)\Big|_{max}\right]^{-1} \tag{4.1}$$

Using a definition of time of max rate of rise differs from the traditional definition for the rise time of a pulse, i.e. the time it takes to transition from 10% to 90% of the maximum value.

As this is the excitation for the system used in this study it is important to understand its spectral content as that will determine the meshing requirements for the

problem. The spectral content is shown to extend out to several THz as is shown in Figure 4.4.
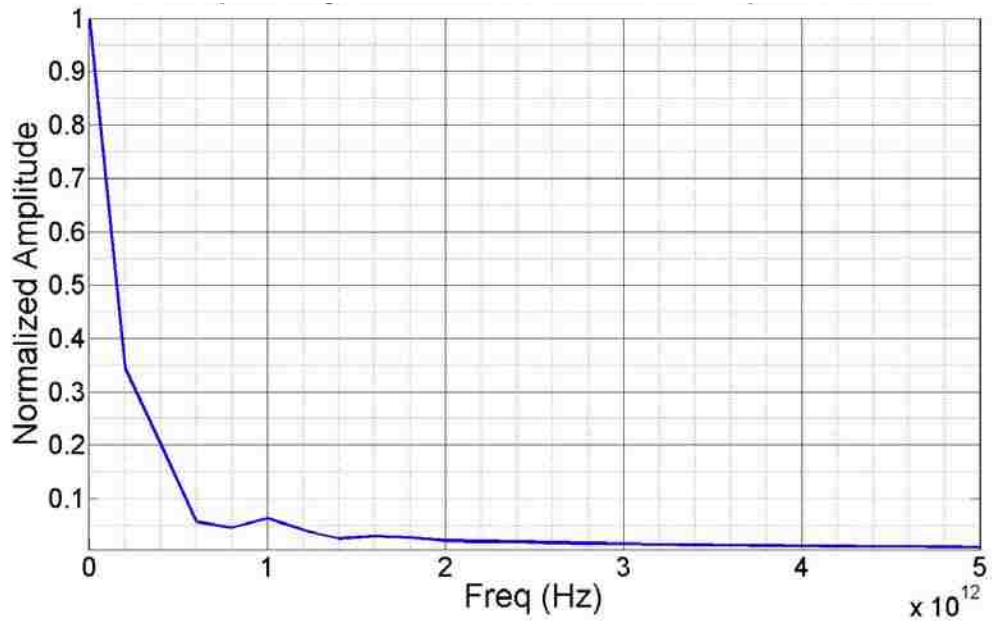
Figure 4.4. Spectral content of SwO input excitation.

The corresponding SwO output is shown in Figure 4.5.
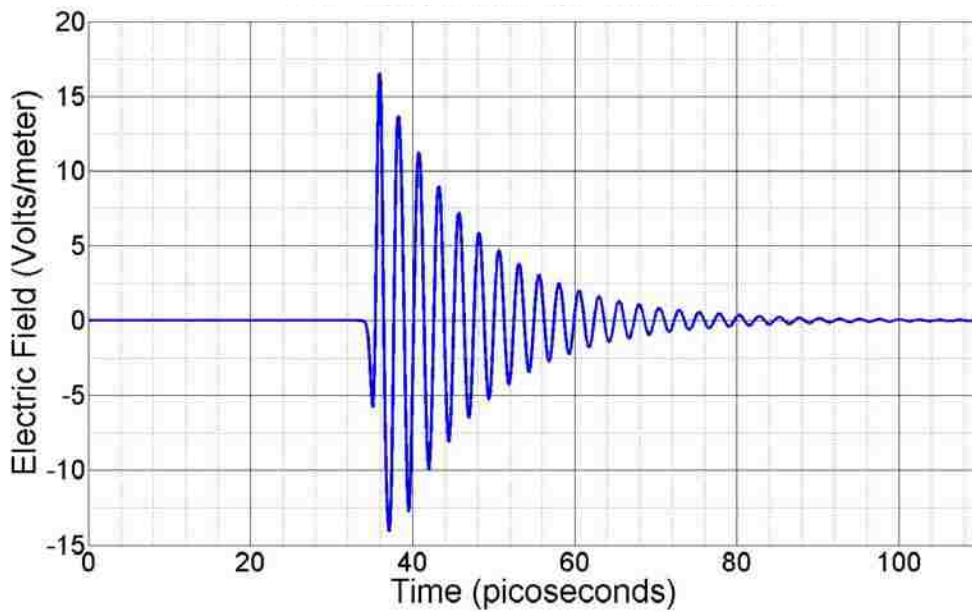
Figure 4.5. Far field electric field probe measurement for SwO.

The damped sinusoidal oscillations that are apparent in Figure 4.5 show multiple facets for what will be considered in designing and optimizing the SwO. First, the peak electric field can be measured from this plot. The Quality factor can be inferred from this plot or the Fourier transform of this data. The Fourier transform of this data also yields a resonant frequency for this structure. Finally, knowledge of the resonant frequency of the structure allows the placement of a far field/RCS monitor that will allow the radiation pattern from the structure to be simulated as well.

The Fourier transform of Figure 4.5 is now shown in Figure 4.6.
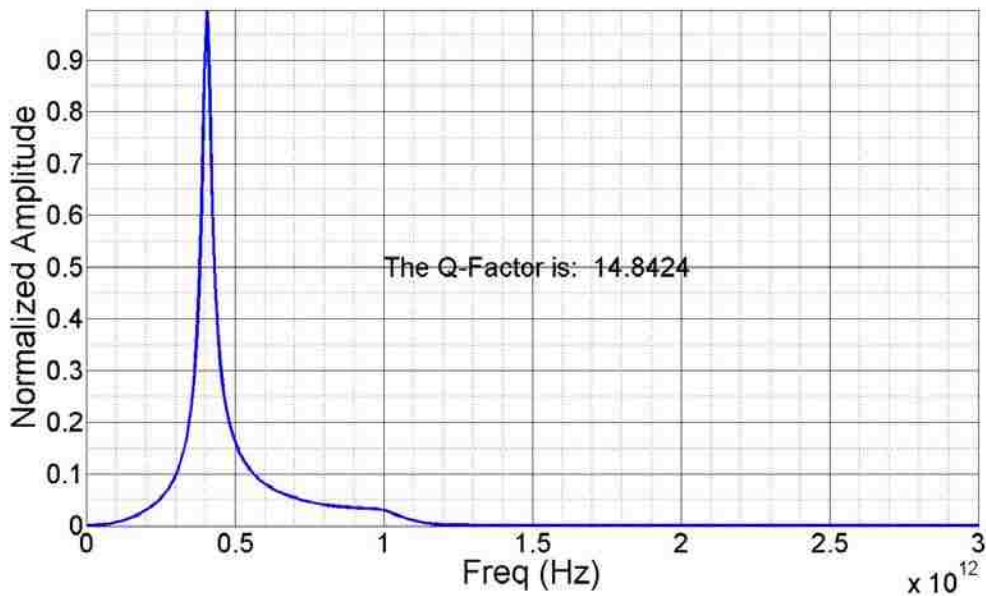
Figure 4.6. Spectral output from SwO.

As is highlighted in Figure 4.5 the Q-factor for the system is measured to be 14.8424 for this data set. The resonant frequency is measured at 0.4056 THz. And finally, this allows the placement of a far field/RCS monitor that is above the SwO at a distance that places the probe in the far field of the device. In this example, the monitor is placed 10 mm above the SwO.

The three dimensional radiation pattern is shown for a frequency of 0.4 THz in Figure 4.7.
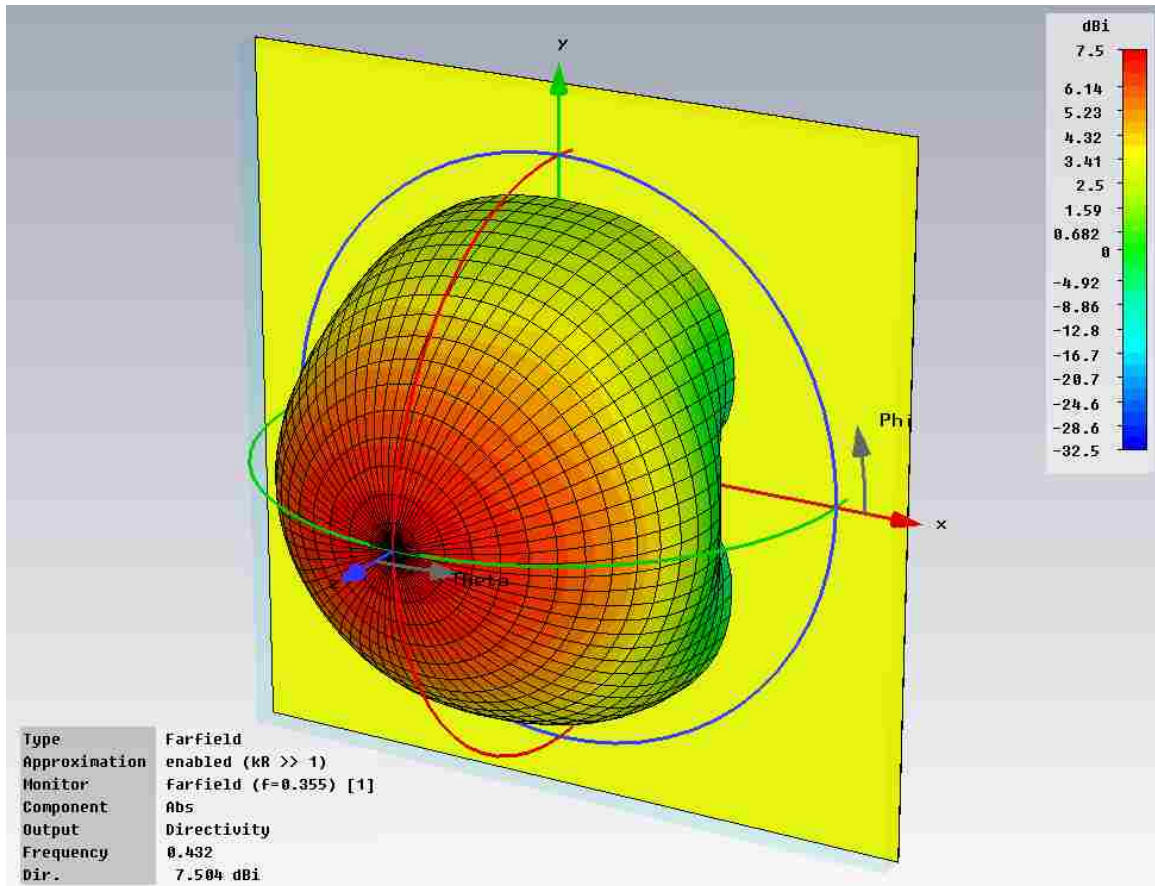
Figure 4.7. Three dimensional radiation pattern for SwO.

The directivity for the 3-dimensional pattern is shown to be 7.504 dBi where dBi is relative to an ideal dipole antenna. In the theta plane the two dimensional radiation pattern can be examined in Figure 4.8.

Directivity Abs (Theta=90)

farfield (f=0.355) [1]

Frequency = 0.432
Main lobe magnitude = 2.2 dBi
Main lobe direction = 295.0 deg.
Angular width (3 dB) = 101.9 deg.

Phi / Degree vs. dBi
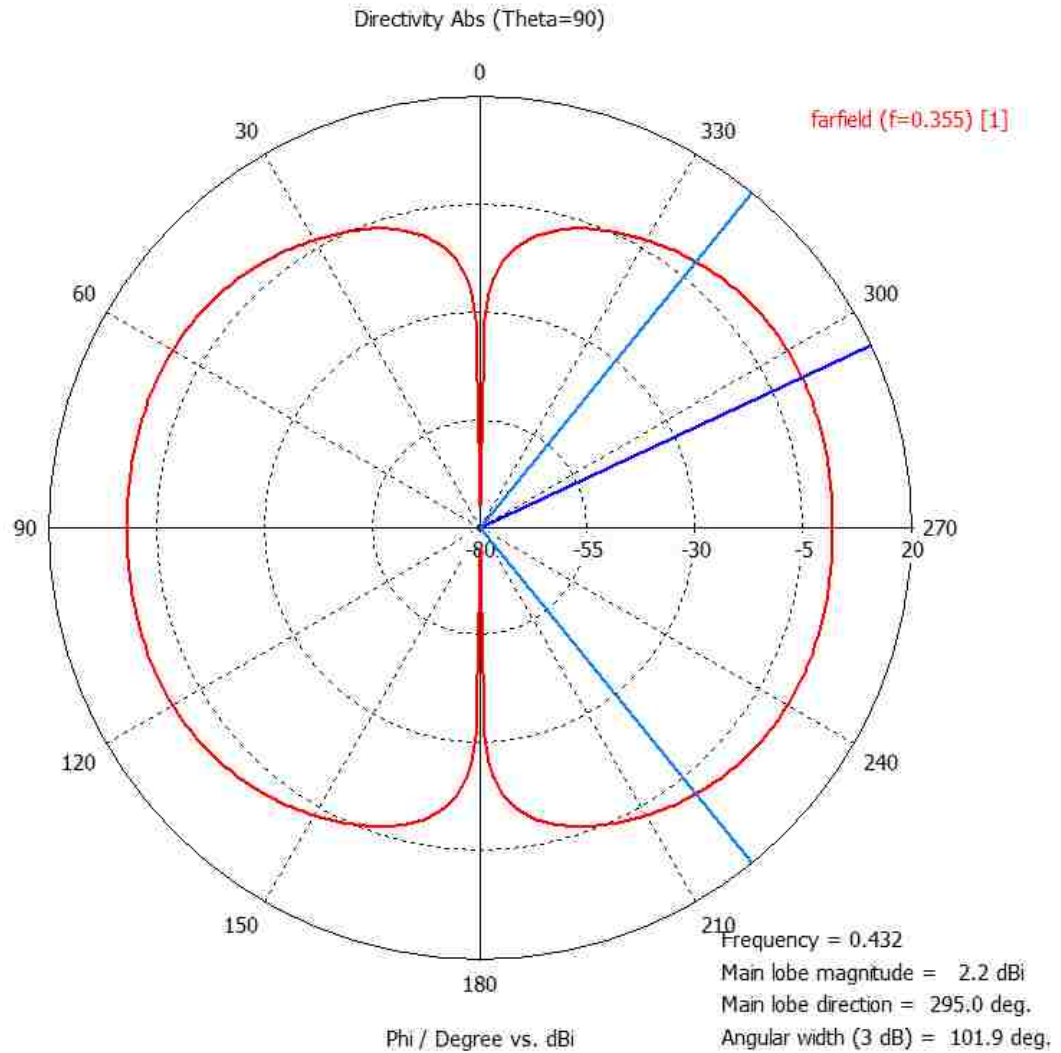
Figure 4.8. Radiation pattern plotted in a polar coordinate system in the theta axis.

This dipolar radiation pattern is what is expected for the output of the SwO and when comparing different design parameters overlaying radiation patterns will help determine the optimum design.

The above examples show what types of analysis will be used for comparing different SwO parameters. This is not an optimized design but is instead a starting place from which the design may be modified.

4.3   Choice of Atmospheric Frequencies for Terahertz Propagation

Historically development in the THz band has been hampered by atmospheric conditions, extremely limiting the range at which propagation has been successfully achieved. The most severe attenuation in the atmosphere may be attributed to water; which for specific harmonics in the THz band can reach attenuation maximums of nearly 10,000 dB/km. With such a response conditions such as humidity, precipitation, and even air turbulence have tremendous impacts on the ability to transmit at the THz band over any significant distance including for communications purposes [15]. Figure 4.9 illustrates how atmospheric attenuation impacts the THz spectrum from 50 GHz to 1 THz.
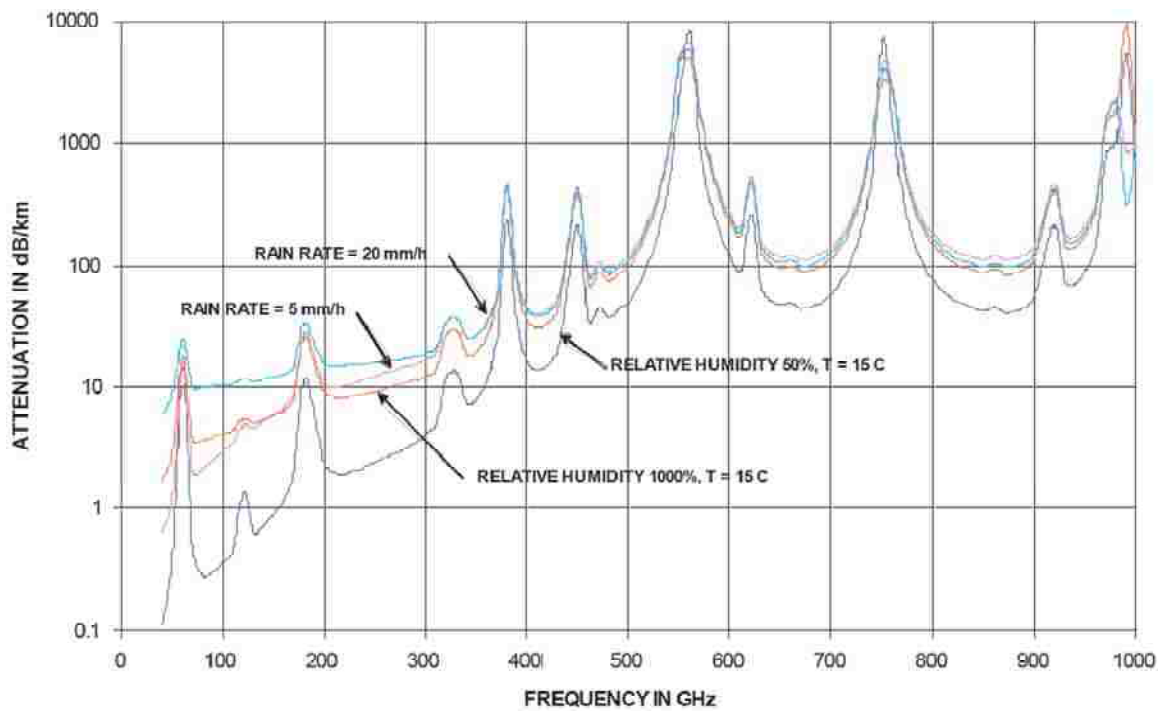
Figure 4.9. Atmospheric attenuation in the range of 40 GHz to 1 THz [15].

Due to these challenges researches have encountered tremendous difficulty in transmitting even a few meters at the higher frequencies where atmospheric attenuation is as much as 500dB/km [15].

Using the troughs in the attenuation curves of Figure 4.9 frequencies of interest are identified that suggest the most favorable points of transmission with regard to attenuation due to atmospheric conditions. These points may be summarized into Table 4.1.

Table 4.1. Attenuation of electromagnetic waves at favorable frequencies [15].

Frequency	Attenuation (dB/kilometer)
80 GHz	0.3 - 4
0.205 THz	2 - 10
0.300 THz	4 - 12
0.405 THz	15 - 30
0.608 THz	50 - 100
0.880 THz	40 - 100

As promising as this discovery is, even optimizing for the identified troughs, using a frequency above 0.6 THz leads to tremendous attenuation. It is clear that for transmission over the greatest distances 0.300 THz is the most reasonable choice for the frequency of operation. The 0.405 THz window also provides an opportunity for distances that are less than a few kilometers [16]. Therefore in final simulated conditions for the SwO a half wavelength leading to 0.300THz will be utilized for these reasons.

4.4   Maximizing the Stored Energy in the Switched Wave Oscillator

The SwO can in essence be seen as a pair of rectangular shaped parallel plate capacitors. The discharge mechanism dictates that the apparent voltage on the pair of plates is twice the stored voltage on a single plate [14]. As such the energy stored quickly reduces to:

$$U_0 = \frac{1}{2} C[2V_0]^2 = 2CV^2 \qquad (4.1)$$

Where U_0 is the stored energy in the SwO, C is the capacitance of the radiators and V is the potential voltage to which the two plates are charged. The primary capacitance in the SwO is found in the energy that is stored between the two rectangular radiators and the ground plane. This electric field is stored within the dielectric that separates these two parallel plates. The final form for the maximum amount of stored energy is shown to be as follows [14].

$$U_0 = 2CV^2 = \frac{\epsilon \omega [l_a - l_s]}{2h} [E_s l_s]^2 \qquad (4.2)$$

Here, ε is the permittivity of the dielectric that separates the SwO from the ground plane, ω is 2πf where f is the operating frequency of the SwO, l_a is the overall length of the SwO, l_s is the length of the switch gap of the SwO, h is the height above the ground plane that the rectangular elements are placed, and finally E_s is the charge voltage to which the SwO is primed. This equation shows that increasing h does increase the stored energy in the SwO, however only to a point. Beyond the condition

$$\frac{h}{l_s} = \frac{E_s}{E_d} \qquad (4.3)$$

the stored energy in the SwO decreases [14].

Maximizing the total stored energy in the SwO is not as simple as maximizing U_0. The radiating condition of the SwO materials must be considered as the photoconductive switch will only be conductive for a finite time. Thus for extremely high values of Q a smaller portion of the stored energy will radiate away in the time that the switch is conductive compared to the case of a SwO with lower Q. A balancing act must then be played in the optimization of the Q-factor for the SwO and the total stored energy in the system.

Chapter 5

Comparison of Simulation Results with Analytical Work

Simulating the specific conditions that have been analytically derived allows for a comparison between the simulation setup and the analytical results. As simulation yields results similar to analysis the simulation domain is shown to be accurate. The ability of simulation to then be used to optimize the SwO is then implied. As correlation is demonstrated, not only can the simulation predict experimental results but can now offer a method to tailor and optimize the performance of the SwO.

Using this approach it is important that each parameter for the design of the SwO be varied independently. This allows for independent analysis of each parameter under scrutiny in the simulation. The distinction of the effect of variation of each individual design characteristic is then clearly demonstrated. From the overall data set of the simulation space an optimum value may consequently be obtained for each individual parameter. It is then extrapolated that the combination of the optimized individual parameters provides an optimized SwO.

In each parameter study, the Q-factor for the system will need to be optimized to the physical geometry. This is due to the fact that the carrier lifetime of the photoconductive switch is finite and will only be conductive for a limited period of time. Thus energy that is not emitted in the period that the switch is conducting is simply not

radiated. After the Q-factor for the study is optimized the peak radiated electric fields may be compared between designs.

Other quantities may also change with the varying of the parameters from the SwO. In particular the resonant frequency is anticipated to change slightly, but for a final design the overall length of the radiators may be adjusted so that the resonant frequency of the SwO is at the desired frequency of transmission.

5.1   Switched Oscillator Height above Ground Plane Parameter Study

The physical height of the SwO above the ground plane is a clear starting point in setting up the simulation domain for a comparison to the derived analytical results. For this set of simulations the initial SwO parameters can be studied with perfect electrical conductors (PEC) and with a vacuum substrate in order to provide an initial case for comparison. This ideal case provides a direct comparison from the simulation domain to the analytical results [14]. The simulation domain may then be expanded to copper radiators and ground planes, but again with an ideal vacuum dielectric, to develop a more realistic simulation for the SwO. The goal will be to optimize the Q-factor for the system such that a design may be developed for a relatively long carrier lifetime.

For this simulation the SwO has the following physical parameters shown in Table 5.1.

Table 5.1. PEC SwO over vacuum varied height simulation space.

SwO Physical Dimension	Microns (μm)
Substrate Height, h	$\lambda_0/20 \geq h \geq \lambda_0/4$
Antenna Length, l_a	$\lambda_0/2 = 300$
Antenna Width, w	$\dfrac{(l_a - l_s)}{2} = 288$
Switch Length, l_s	$\dfrac{\lambda_0}{50} = 12$
Thickness of SwO	1
Thickness of Ground Plane	1
Substrate and Ground Plane Length	$3\lambda_0 = 1800$
Substrate and Ground Plane Width	$3\lambda_0 = 1800$

Where λ_0 is the wavelength in free space and λ is the wavelength in the dielectric..

The physical simulation space is shown in Figure 5.1 and as one would expect it appears very similar to Figure 4.1.
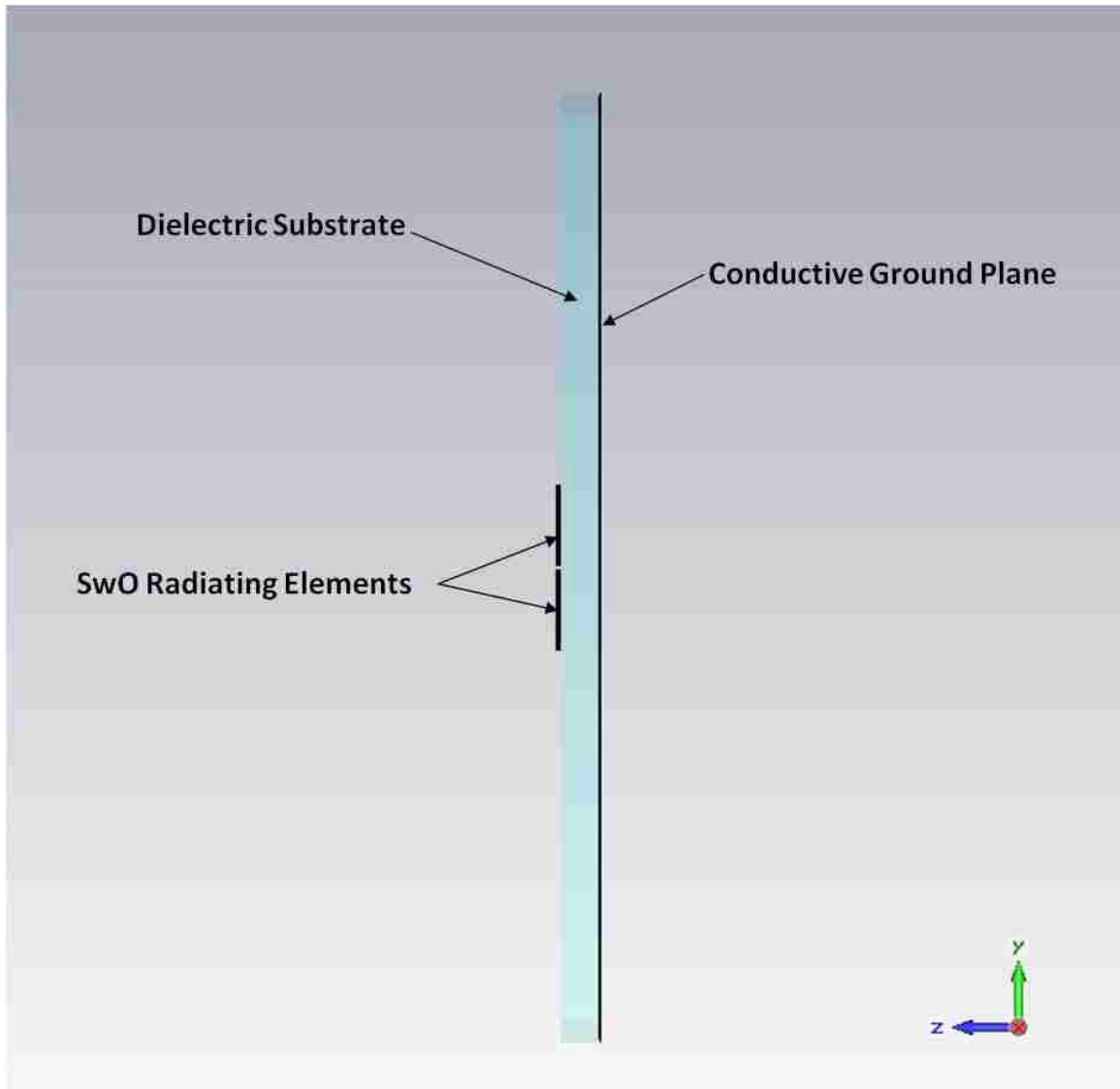
Figure 5.1. SwO varying height simulation setup.

For this simulation the height of the SwO dielectric thickness is set, and then the simulation is run using the time domain solver. After the simulation for this set of parameters is completed the height is set to a new value and the simulations run again, and so forth until the simulation space is satisfied.

The results of each simulation are more readily interpreted when all units are in terms of the height divided by lambda so that the end result is dimensionless. Also, by keeping the various heights in terms of lambda, when a realistic dielectric is used in

simulation the dimensionless analysis provides direct comparison between data. An analysis of equivalent heights would not provide this comparison due to the dependence of the length of lambda on the substrate.

The results of the first simulation sweep, with PEC conductors in vacuum, are summarized in Table 5.2.

Table 5.2. PEC and vacuum SwO vs. height.

h / λ	E_{max} (V/m)	F_0 (THz)	Q-Factor
0.050	35.135	0.338	84.803
0.075	41.936	0.339	43.638
0.100	46.399	0.338	27.467
0.125	48.988	0.334	19.439
0.150	50.202	0.332	14.740
0.175	50.573	0.375	11.764
0.200	49.838	0.372	9.656
0.225	47.953	0.370	8.154
0.250	44.983	0.367	7.012

The resonant frequency of the SwO does shift on the order of ± 4% throughout the simulation sweep. Also, the stored energy in the SwO increases as the height above the ground plane is decreased. This is due to a direct increase in the stored capacitive energy between the radiating elements of the SwO and the ground plane.

Due to the use of PEC and vacuum this case allows a direct comparison to the derived analytical results. Analytical results for two distinctly different cases are available for which comparisons may be made to this simulation set.

Case 1: $h/\lambda = 0.25$; $\qquad Q \approx \frac{\omega[l_a - l_s]}{h l_a}$ $\qquad\qquad$ (5.1)

By applying the defined parameters of the simulated case to the relation a Q-factor of 0.96 would be anticipated. However, this significantly differs from the Q-factor calculated by the simulation which yields 7.012. This discrepancy isn't entirely unexpected. There are many differences between analysis and simulation that may account for the difference, specifically assumptions that must be made so the problem lends itself to a closed form solution. It is assumed in analysis that the fringe fields will not significantly impact the overall radiated field and therefore their effect may be ignored. The second is that the analytical results are calculated by assuming a previously known current distribution for the dipole moment at the resonant frequency. Lastly, the analytical results are derived on a unit step input to the SwO where this cannot be physically realized nor is it a condition that can be simulated [16].

The second case that is derived is for that of a height of less than $\lambda/20$, or $h \ll \lambda$.

Case 2: $\qquad h/\lambda = 0.05; \qquad Q \approx \frac{15}{64\pi} \left[\frac{l_a}{h}\right]^3$ $\qquad\qquad$ (5.2)

Where Q is the quality factor, l_a is the overall length of the radiator, and h is the SwO height above the ground plane [16]. Applying this relation to the simulated cases gives a Q of 74.60. Comparing to the simulated Q of 84.803 shows that these two values are in reasonable agreement. The Q-factors that have been analyzed in both the PEC and copper cases are plotted in Figure 5.2.
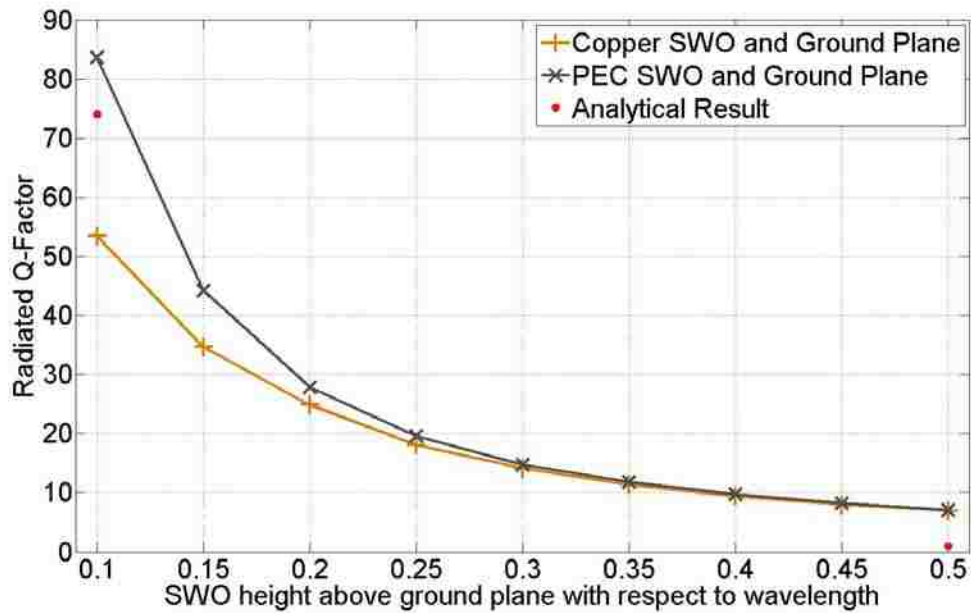
Figure 5.2. SwO vs. height for PEC, copper, and analytical.

What is shown by comparing the different cases is that the Q-factor for the SwO increases exponentially as the substrate height decreases. It can also be observed that when simulation and analytical results are overlaid there is some correlation between them. While there are only two points shown from the analytical approach as there are only two clear cases that are derived the relative differences at the points for which analysis has been performed show agreement and suggest a trend obtained in decreasing the height of the SwO.

The Q of the system is greatest at the smallest simulated heights. However, Q is only a single factor for the total system performance. In the height simulation it is also critical to verify the radiation patterns for the simulated data hasn't deviated from a dipole pattern. Also, for this comparison it is only relevant to consider the case of copper radiators and ground planes as they are physically realizable as opposed to PEC. Plotting the various normalized radiation patterns for the SwO on top of each other show that in each case the device is radiating in a dipolar pattern as intended. This is shown in Figure 5.3.

48
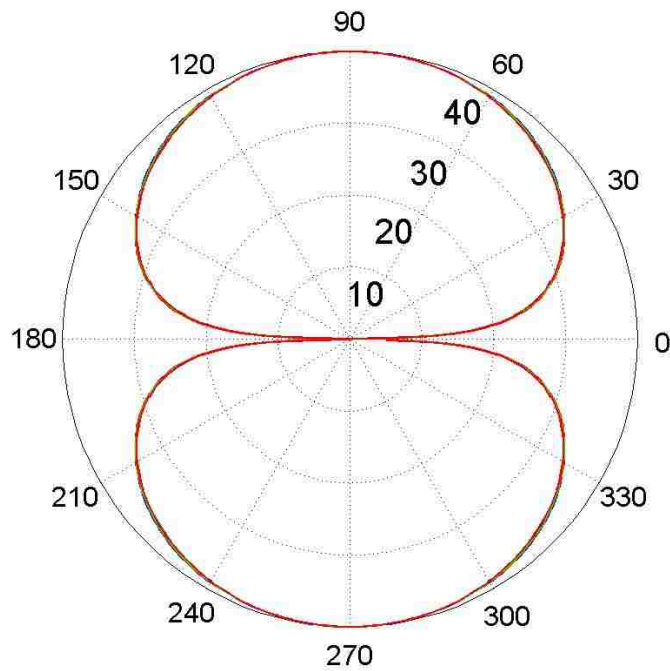
Figure 5.3 SwO normalized directivity radiation patterns.

What is learned from this simulation is that Q is maximized when $h \ll \lambda$ and that varying the height of a design does not significantly impact the radiation pattern of the SwO. This outcome is very important in the development of optimized SwO parameters as the height of the device may be used to tailor the Q, either to increase or decrease the radiated Q, so that the best design may be obtained. If there is an attractive photoconductive material with much shorter carrier lifetime a lower Q will be required so that the stored energy within the device may be radiated within the active period of the switch. Conversely a photoconductive material with longer carrier lifetime would perform best in a design with a higher Q-factor. Thus the value of Q may be utilized and the radiated power density be designed to the switch material.

49

5.2   Switched Oscillator Substrate Permittivity Parameter Study

The next parameter to be systematically varied is the substrate permittivity in   the transmitting system. For this simulation a substrate height of λ/8 is chosen as it presents a high Q-factor and good radiation characteristics. It is important to understand that the length of the SwO and the height above the ground plane are based on the wavelength *in the substrate*. For a vacuum substrate, there is no difference between the wavelength in air vs. the wavelength in the dielectric. However, when using a dielectric the length of the SwO and the height must be scaled according to the dielectric's permittivity. This is accomplished by determining the ratio between the wavelength in vacuum and the wavelength in the dielectric. This is done with (5.3).

$$\lambda = \frac{\lambda_0}{\sqrt{\varepsilon_r}}$$

(5.3)

Where λ_0 is the wavelength in vacuum, ε_r is the relative permittivity of the dielectric, and λ is the wavelength in the dielectric. By using this relationship the physical dimensions of the SwO can be individualized to a dielectric to maintain consistent height and length in terms of wavelength.

It is important to note that as the relative permittivity of the substrate is increased, the overall dimensions for the area of the SwO decrease by the inverse of the root of the relative permittivity. The overall height of the SwO mirrors this effect.

For this portion of the study the antenna width is set to be half of the overall length of the radiator. The charge voltage and gap spacing are also held constant. This means the energy stored in the SwO is proportional to the capacitance of the system. The capacitance of the device is therefore:

$$C = \varepsilon \frac{S}{h} \approx \varepsilon_0 \varepsilon_r \frac{\left[\frac{\lambda_0}{2\sqrt{\varepsilon_r}}\right]\left[\frac{\lambda_0}{4\sqrt{\varepsilon_r}}\right]}{\left[\frac{\lambda_0}{8\sqrt{\varepsilon_r}}\right]} = \varepsilon_0 \sqrt{\varepsilon_r} \lambda_0 \qquad (5.4)$$

Where C is capacitance, ε is the permittivity of the dielectric, S is the surface area, ε_0 is 8.854×10^{-12} F/m, and all other parameters have been previously defined.

This leads to the conclusion that over the simulation space higher dielectric constants yield a SwO with more stored energy than does a SwO with lower dielectric constants. The definition of simulation parameters are shown in Table 5.3.

Table 5.3. Substrate permittivity simulation space.

SwO Physical Dimension	Microns (μm)
Substrate Relative Permittivity	2 - 10
Substrate Height, h	$\lambda/8 = \lambda_0 / (8\sqrt{\varepsilon_r})$
Antenna Length, l_a	$\lambda/2 = 600 / (2\sqrt{\varepsilon_r})$
Antenna Width, w	$\dfrac{(l_a - l_s)}{2}$
Switch Length, l_s	$\dfrac{\lambda}{50}$
Thickness of SwO	1
Thickness of Ground Plane	1
Substrate and Ground Plane Length	$3\lambda_0 = 1800$
Substrate and Ground Plane Width	$3\lambda_0 = 1800$

For all values of relative permittivity, the substrate is assumed to be ideal. The assumption of a lossless dielectric is valid for this simulation as there is not yet an identified substrate material from which to construct the SwO.

The sweep results for the maximum electric field value, resonant frequency, and Q are summarized in Table 5.4.

Table 5.4. SwO vs. substrate permittivity.

ε_r	E_{max} (V/m)	F_0 (THz)	Q-Factor
2	37.764	0.355	18.240
3	32.269	0.437	17.953
4	28.181	0.506	17.683
5	25.487	0.570	17.146
6	22.680	0.626	16.608
7	20.488	0.677	16.506
8	18.638	0.725	16.232
9	16.981	0.771	15.886
10	15.470	0.813	15.759

It is clear that the radiated Q of the SwO is nearly constant over the simulation domain. The table also shows that the resonant frequency of the SwO increases with the relative permittivity of the substrate. The values of relative permittivity vs. resonant frequency are plotted in Figure 5.4.
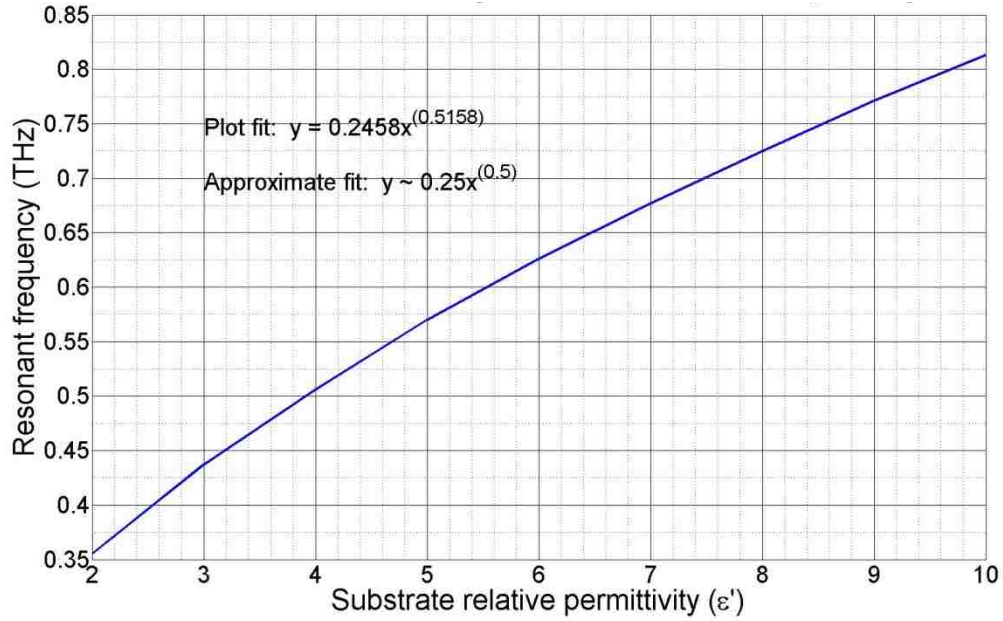
Figure 5.4. resonant frequency vs. relative permittivity.

There is a very elegant fit for the plotted curve of resonant frequency vs. the substrate relative permittivity that is shown in Figure 5.4. This relation is shown in (5.5).

$$f_0 = \frac{\sqrt{\varepsilon_r}}{4} \qquad (5.5)$$

The design rule of (5.5) holds for similar SwO designs where f_0 is the resonant frequency in THz. This relation is expected because the length of the SwO was scaled so that the overall dimensions with respect to the dielectric remained constant. However the length was adjusted inversely with $\sqrt{\varepsilon_r}$ per (5.3), while the capacitance is proportional to $\sqrt{\varepsilon_r}$ per (5.4). Therefore the effect of the permittivity on the capacitance is cancelled. The net result is that for SwO designs operating at the same frequency using different substrates, the stored energy between the two will stay nearly identical.

While the energy that is stored within the SwO stays constant between designs of differing permittivity and identical resonant frequency, the overall radiation efficiency decreases as the stored energy in the SwO is more tightly coupled in substrates with

higher dielectric strengths. Higher dielectric constants also exhibit greater tendency for energy loss in dielectric waves [17]. For this reason, it is clear that an optimum substrate for the SwO will have as low a dielectric constant as possible. For this reason, polyethylene may make a very reasonable choice as it has a relative permittivity of ~2.25, is readily available in thin films, and has potential to have the radiators mated to the material through Chemical Vapor Deposition (CVD). The idea of using polyethylene is further developed in Chapter 6.

As with substrate height the radiated power patterns are plotted in Figure 5.5 to show that the dipolar pattern remains constant.
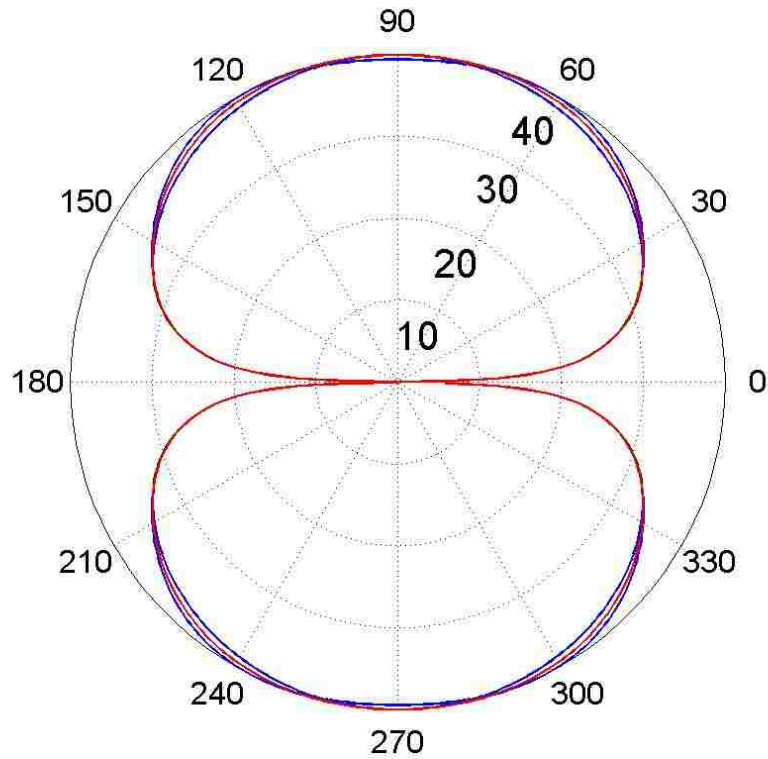
Figure 5.5. SwO normalized directivity radiated power pattern vs. relative permittivity.

5.3   Switched Oscillator Width Parameter Study

In simulations so far the width of the SwO has been held constant at just less than $\lambda/2$. This is done to prevent a potential second resonance, of twice the fundamental, operating in the width dimension of the SwO. In this section the width of the SwO will be varied to ascertain a single optimum design width.

For this simulation the substrate height will be fixed at $\lambda/8$ per the results of section 5.1 and the substrate material will be selected to be a lossless polyethylene with a relative permittivity of $\varepsilon_r = 2.25$ per the results of section 5.2. The simulation parameters are shown in Table 5.5.

Table 5.5. SwO width simulation space.

SwO Physical Dimension	Microns (µm)
Substrate Height, h	$\lambda_0 / (8\sqrt{\varepsilon_r}) = 50$
Antenna Length, l_a	$\lambda / (2\sqrt{\varepsilon_r}) = 200$
Antenna Width, w	$\lambda / 20 \leq w \leq \lambda$
Switch Length, l_s	$\frac{\lambda}{50} = 8$
Thickness of SwO	1
Thickness of Ground Plane	1
Substrate and Ground Plane Length	$3\lambda = 1200$
Substrate and Ground Plane Width	$3\lambda = 1200$

By increasing the width with a fixed length capacitance will vary proportional to the area of the radiators per equation 5.4. That being stated, the results of the simulation are summarized below in Table 5.6..

Table 5.6. SwO vs. radiator width.

w / λ	E_{max} (V/m)	F_0 (THz)	Q-Factor
0.050	16.919	0.466	15.553
0.100	22.174	0.437	15.502
0.125	24.900	0.424	15.733
0.150	27.911	0.413	16.074
0.200	33.140	0.392	17.023
0.250	36.116	0.378	18.039
0.300	38.820	0.356	20.059
0.350	39.643	0.340	22.066
0.400	39.593	0.324	24.030
0.450	39.051	0.310	26.295
0.500	38.007	0.295	28.277
0.625	33.961	0.266	33.444
0.750	28.764	0.240	38.214
0.875	23.951	0.217	44.363
1.000	20.246	0.199	48.615

The table shows that as the width of the radiator is increased, the resonant frequency decreases, and the Q of the system increases. The resonant frequency vs. SwO width is plotted in Figure 5.6.
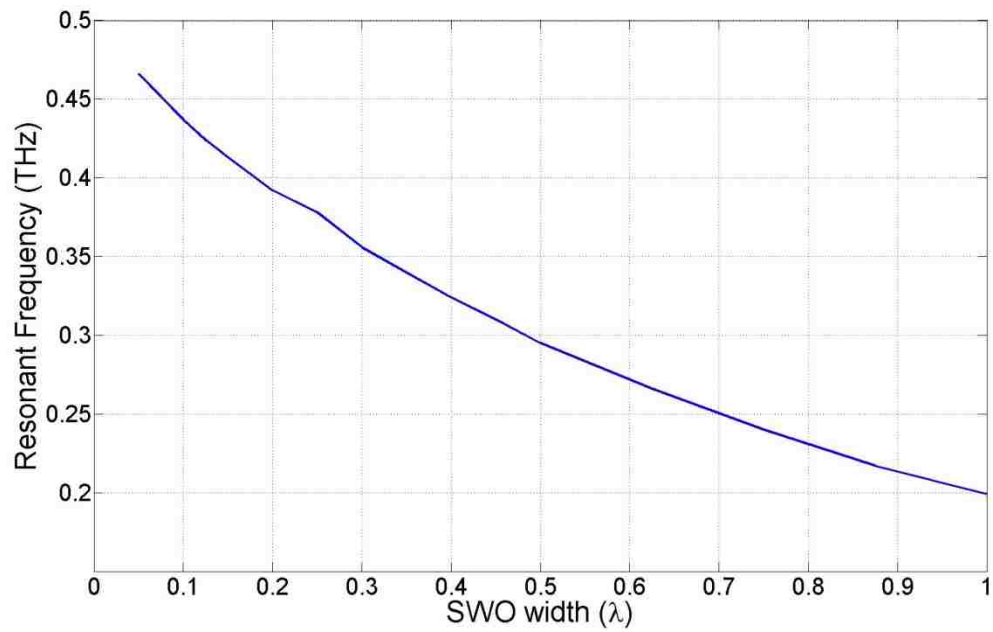
Figure 5.6. SwO width vs. resonant frequency.

It can be concluded from this data that the wider the radiating elements in the SwO the longer they appear electrically. The Radiated Q-factor vs. SwO width is plotted in Figure 5.7.
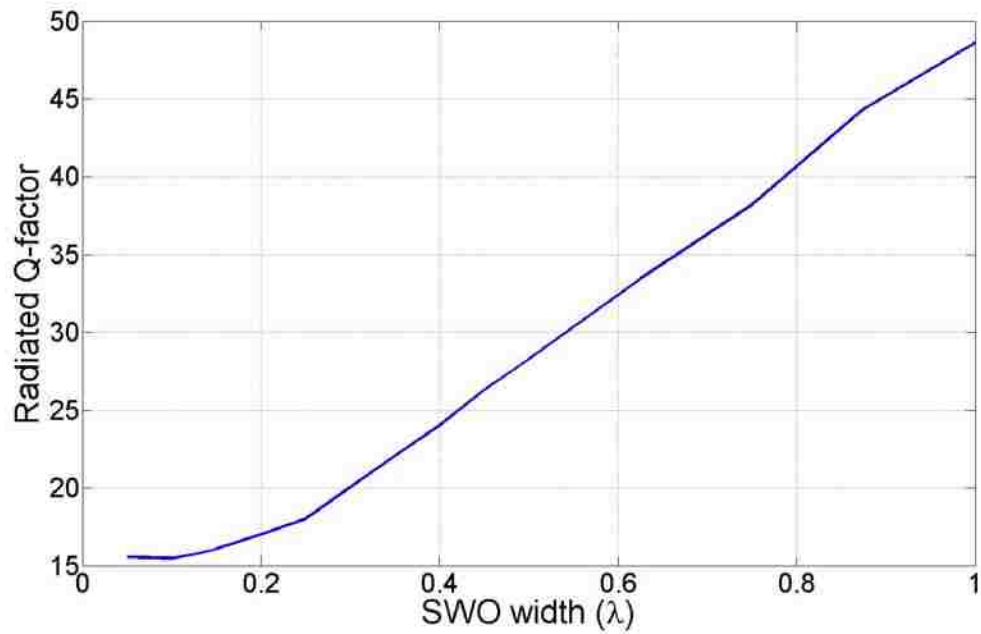
Figure 5.7. SwO width vs. radiated Q-factor.

The radiated power density is what is found to be the discriminating factor for this simulation. For this analysis, the two dimensional radiation pattern is plotted in Figure 5.8 for the instances of greatest radiated power density.
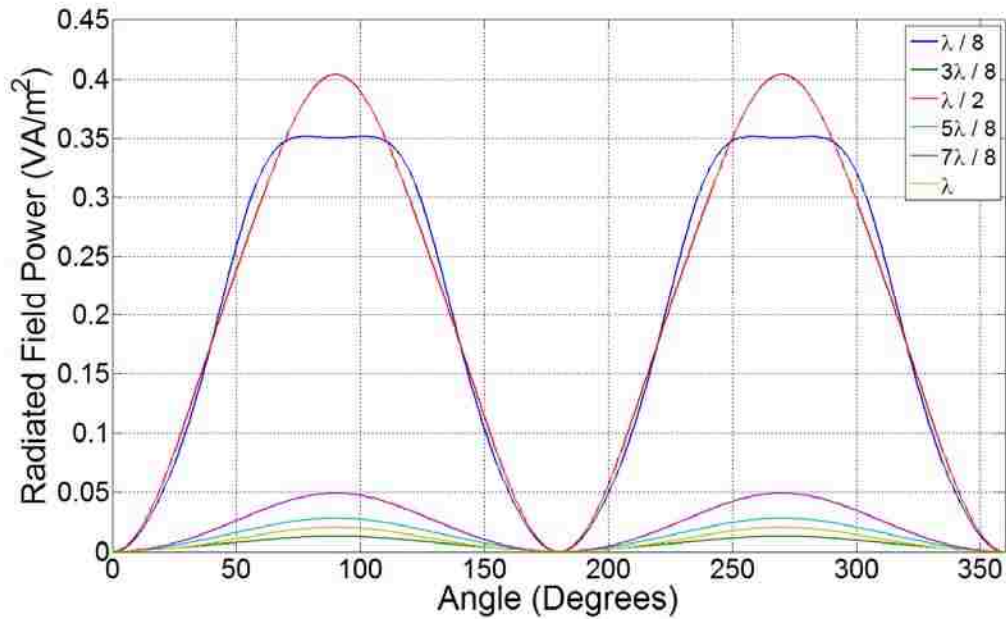
Figure 5.8. SwO radiated power density vs. width.

Smaller SwO widths are less likely to be capable of harboring higher order modes than the fundamental resonance. Higher order modes detract from the SwO pushing the majority of the stored energy in the radiators in a single narrow band emission. Therefore while the case of highest radiated power density is $\lambda/2$ at this width the structure will be most likely to carry a higher order mode. For this reason we will look to the next highest radiated power density, in this case it is $\lambda/8$. Due to decreased capability of the narrower design of supporting higher order modes a SwO width of $\lambda/8$ is chosen as the optimum case.

5.4   Switched Oscillator Switch Gap Length Parameter Study

The length of the switch gap is subject to competing interests. The first being that a smaller gap will have better switching performance. The shorter switch has less resistance as well as decreased current loss, increasing the energy available to the

59

radiating geometry of the SwO. However, longer switch gaps allow a higher charge voltage to be attained across the two plates. The energy that is stored in the SwO is proportional to the square of the charge voltage. This leads to the necessary understanding of what benefits and downfalls occur with various gap spacing in order to optimize this parameter.

The simulation parameters for this optimization study are shown in Table 5.7.

Table 5.7. SwO switch gap simulation space.

SwO Physical Dimension	Microns (μm)
Substrate Height, h	$\lambda_0 / (8\sqrt{\varepsilon_r}) = 50$
Antenna Length, l_a	$\lambda / (2\sqrt{\varepsilon_r}) = 200$
Antenna Width, w	$\lambda / (4\sqrt{\varepsilon_r}) = 100$
Switch Length, l_s	$\frac{\lambda}{50} \leq l_s \leq \frac{\lambda}{5}$
Thickness of SwO	1
Thickness of Ground Plane	1
Substrate and Ground Plane Length	$3\lambda = 1200$
Substrate and Ground Plane Width	$3\lambda = 1200$

As has been the approach for each section of the simulation study, all values are held constant while varying a single parameter. For this reason the larger charge voltages that are possible with larger switch gap lengths are not taken into account. The far field values obtained in simulation may be scaled to account for the higher charge voltages after it is known what maximum voltages can be achieved with different gap spacing. The results of the simulation are summarized in Table 5.8.

Table 5.8. SwO vs. switch gap length.

l_s / λ	E_{max} (V/m)	F_0 (THz)	Q-Factor
0.020	41.298	0.390	15.003
0.040	36.819	0.374	18.517
0.060	33.695	0.361	21.200
0.080	30.612	0.350	24.315
0.100	27.993	0.339	28.028
0.120	25.929	0.331	29.798
0.140	21.033	0.324	32.912
0.160	22.290	0.317	35.245
0.180	20.778	0.311	37.517
0.200	19.374	0.305	39.059

The table shows that as the switch length is increased the radiated Q-factor also increases while the resonant frequency decreases. The radiated Q-factor is displayed in Figure 5.9.
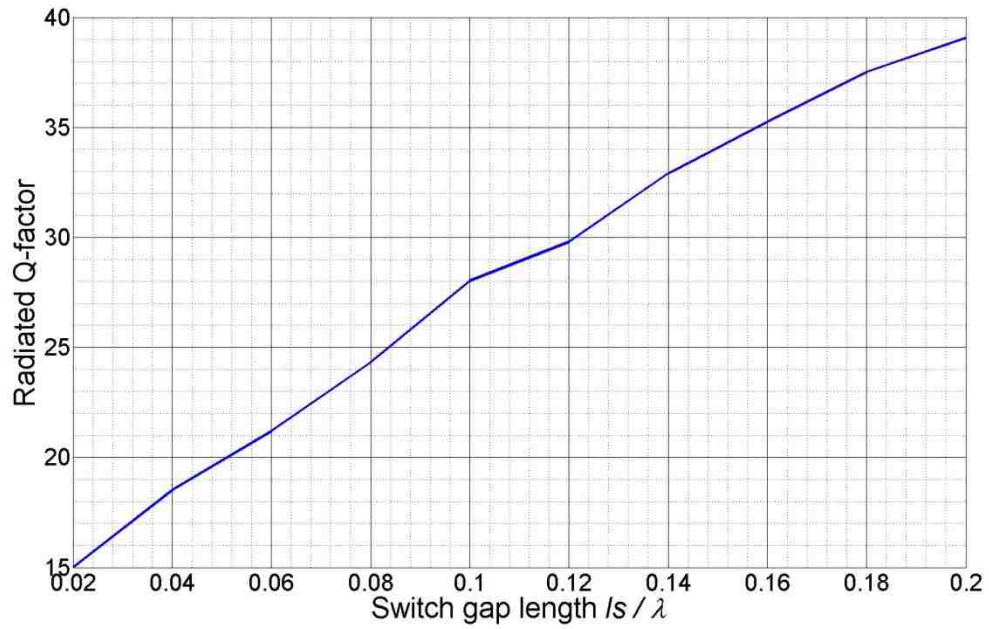
Figure 5.9. SwO switch length vs. radiated Q-factor.

The increase in the radiated Q is representative of there being less loss in the system. As the switch gap is made larger, the total area of the copper radiators is decreased leaving the ratio of the overall SwO length of copper radiators to switch length lower. The effect of increasing l_s on a fixed l_a can be seen in Figure 4.2. In simulation the switch is defined as lossless, so an analysis error could occur if the increasing Q were due to loss decreasing because of the reduction in the overall surface area, and therefore resistance, of the radiators. If this were the case then PEC with a small gap should have a Q-factor similar to that of copper with a large gap. However, the Q-factor for the SwO when simulated from PEC radiators and a copper ground plane yields a value of 16.223 at a switch length of 0.02 compared to 39.02 for copper at 0.2 clearly indicating that this is not the case. The net result is that the Q for the SwO may be increased with the larger gap spacing that may be required at higher charge voltages.

The second consideration is the resonant frequency of the SwO for gap length as illustrated in Figure 5.10.
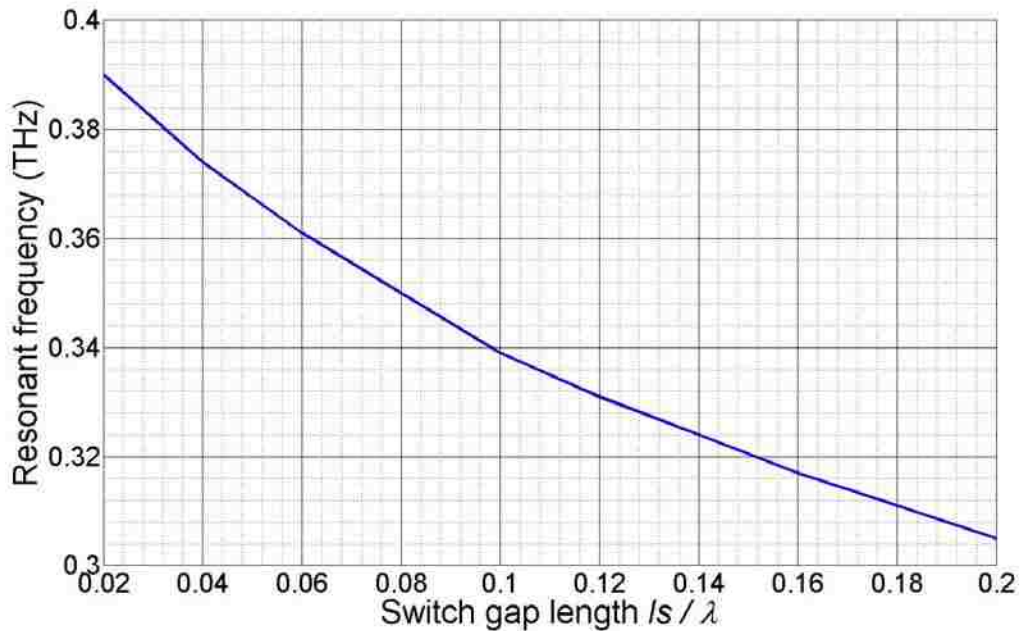
Figure 5.10. SwO switch length vs. resonant frequency.

The resonant frequency of the SwO is shown to decrease as the radiating portion of the antenna is decreased by the intruding length of the switch. This makes the overall electrical length of the SwO shorter in simulation. Practically, however, the overall length of the SwO is not changing. It will be important to compare experimental results with this simulation set to ensure accuracy.

Chapter 6

Results

Compiling what was learned in the simulation of the various SwO parameters into a single design creates a final optimized design that can be built and experimentally tested by UTOL. For this, all of the optimized parameters for the SwO will be combined and simulated so that an immediate comparison of experimental and simulated results may be made. Findings from the simulated cases may also be summarized as general rules for optimizing the design of a SwO at THz frequencies.

6.1 Simulated Relationships

In comparing Q-factors of different designs it is important to remember that the Q is a ratio of the energy stored in the SwO to the loss per cycle for the SwO. This translates into high Q designs taking longer to radiate the energy that is stored in the SwO. The Q of the SwO is an important design factor because if the Q for the system leads to an extremely long time for the stored energy to be radiated, the finite time the photoconductive switch is active will truncate how much energy is emitted by the SwO. A low Q-factor on the other hand is representative of a device that has a wider spectral emission. A wider spectral emission is less advantageous for communications because

atmospheric conditions severely attenuate the signal. Having a wider spectral emission leads to a lower Power Spectral Density (PSD) for a single frequency as the stored energy in the device is not being focused as well into the transmission wavelength.

The simulation set described in section 5.1 illustrated that decreasing the substrate height for the SwO increases the stored energy in the device and raises the Q-factor at which the SwO radiates. Using the simulated values for radiated power density there is a tremendous advantage in using a substrate height that is less than 10% of the wavelength in the dielectric. As photoconductors of interest for the SwO are considered it is anticipated that the carrier lifetime of the switch will be between 50 and 100 ps. The Q-factor determines how many cycles of the signal may be emitted for a given design. The frequency of the carrier can then be used with that number of cycles to determine the carrier lifetime required. A SwO design will need to be made such that the majority of the stored radiation may be emitted within the conductive time of the switch.

Since the medium necessary for communication applications is air the ideal dielectric for the SwO is vacuum, or air, as they do not couple fields between the ground plane and the SwO any tighter than fields that are radiated due to the absence of impedance discontinuity. Of course this is not a feasible condition due to the requirement for a solid material for support. LT-GaAs presents perhaps the most easily manufacturable substrate because the SwO and ground plane may be directly etched on the photoconductive switch. However it also possesses a relative permittivity of ~12.9. This is prohibitively high making this solution undesirable.

The substrate of choice must be one that has low relative permittivity and exhibits good manufacturing capability. Polyethylene presents an opportunity. It is possible to take advantage of a common material with a relative permittivity of ~2.25 that also comes readily available in thicknesses as small as 0.0005", but also larger. A half mil thickness lends itself to a substrate height of $h/\lambda \approx 1/32$; since this is well below the goal of 10% of the wavelength this is an acceptable dielectric choice as it allows for an optimized height for the SwO. It is also easily applied to this application through use of standard thin film technologies. Using a substrate of polyethylene a SwO design may be constructed using chemical vapor deposition to build the metallic radiators and ground

plane directly on the thin film. For this reason, initial optimized SwO designs will be done using the parameters of polyethylene.

The simulation set described in section 5.3 found that the optimum width for the SwO is $\lambda/8$. This value is chosen over a value of $\lambda/2$ though $\lambda/8$ has a lower radiated power density. The width of $\lambda/8$ is chosen because of its lower propensity to allow higher order modes to propagate across the SwO. This gives a firm value for the width of future SwO: for polyethylene at the design frequency of 0.4 THz this width is 50 µm.

With regard to physical fabrication of a SwO for validation of the simulations described herein, an initial switch gap length of 10 µm is used. This value is chosen as it is a common spacing for test antennas fabricated at UTOL. This spacing is known to hold off charge voltages of 60 volts. The optimum switch gap length will require further analysis that can incorporate the associated breakdown voltages. This study would incorporate the dynamic relationship between the gap spacing, charge voltage, stored energy, and radiated power density. This is discussed in further detail in Chapter 7.

6.2   Development of Switched Oscillator on Polyethylene

The design parameters discussed in Chapter 5 were varied and optimized independently. However they can now be combined to form a complete SwO design that, by incorporating all optimized parameters, is itself optimized. This design in toto can then be simulated within CST. The simulation of the final conditions is intended to predict what an experimental setup will produce. The parameters for this optimized design are summarized in Table 6.1.

Table 6.1. First optimized SwO physical geometry.

SwO Physical Dimension	Microns (µm)
Substrate Height, h	12.7
Antenna Length, l_a	$\lambda / (2\sqrt{\varepsilon_r}) = 200$
Antenna Width, w	$\lambda / (8\sqrt{\varepsilon_r}) = 50$
Switch Length, l_s	10
Thickness of SwO	1
Thickness of Ground Plane	1
Substrate and Ground Plane Length	$3\lambda = 1200$
Substrate and Ground Plane Width	$3\lambda = 1200$

These physical characteristics lead to a narrower SwO than has been previously depicted in this thesis. Figure 6.1 shows the general size relationships of this SwO.
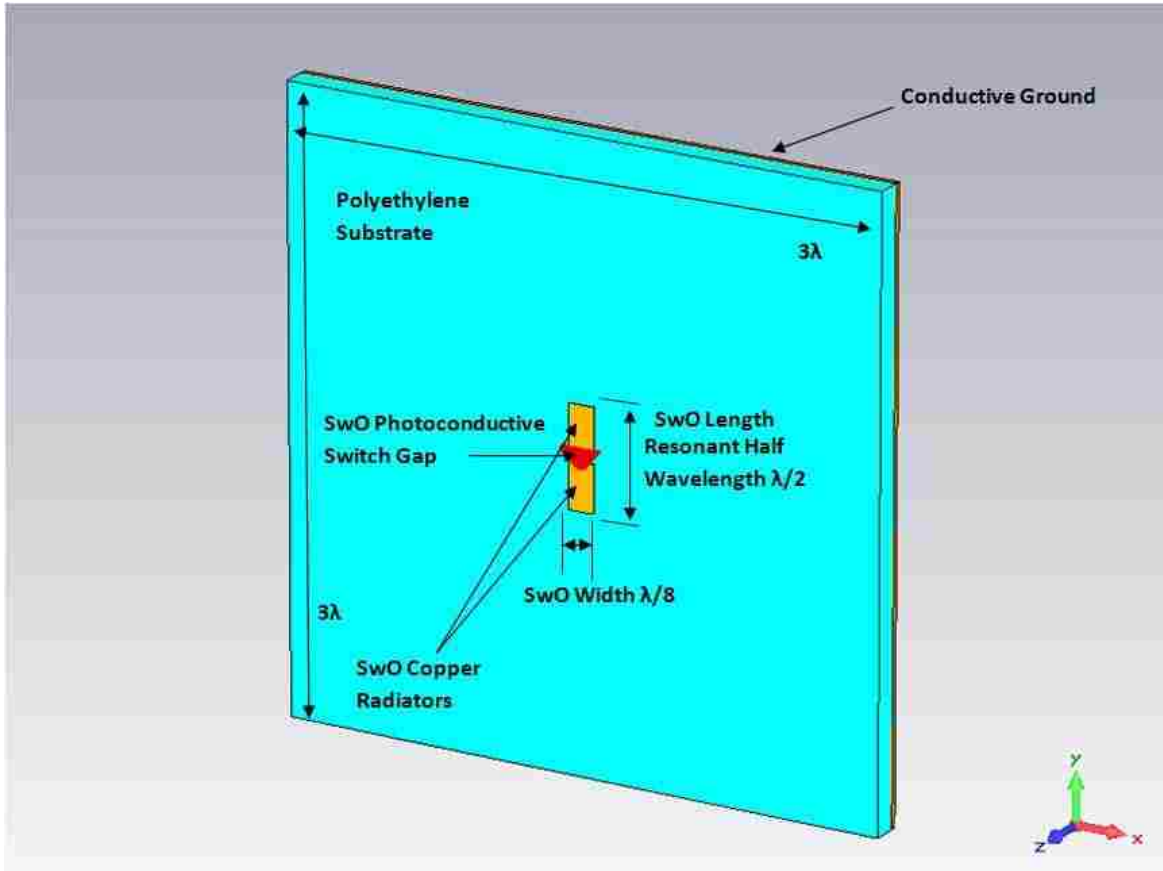
Figure 6.1. Optimized SwO.

The performance of the optimized SwO is listed below in Table 6.2.

Table 6.2. First optimized SwO performance summary.

SwO Performance Characteristic	Simulated Value
Resonant Frequency	0.4108 GHz
Q-Factor	68.846
E_{max} (V/m)	13.954 V/m

The radiated Q-factor for this design is quite high. In plotting the simulated electric far field probe data it is clear that the Q for this design is too large because it

takes nearly 300 ps for the stored energy in the device to radiate away. The electric far field probe data is shown in Figure 6.2.
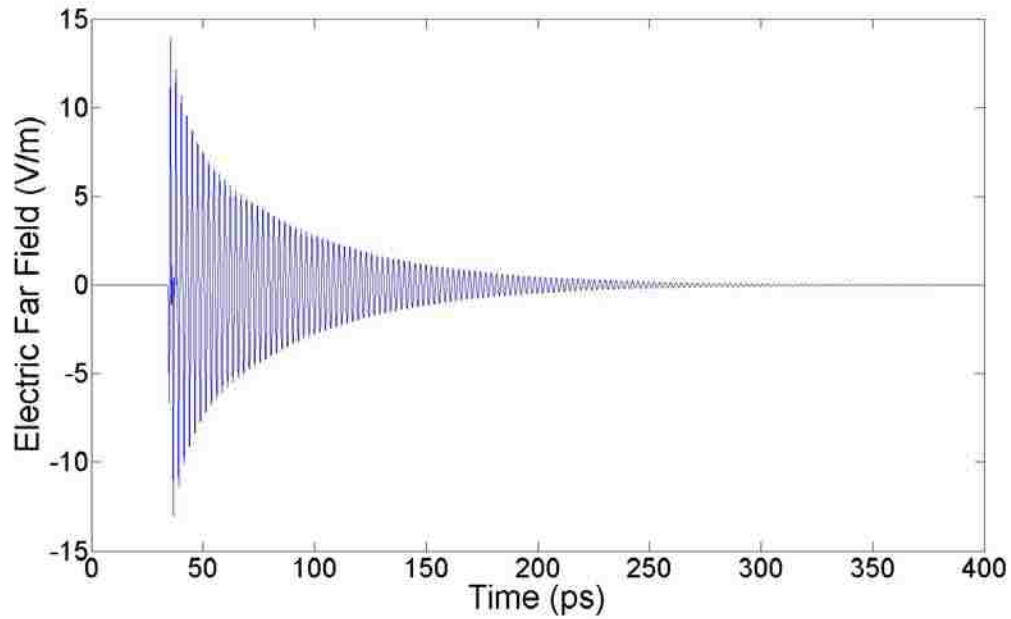
Figure 6.2. Electric far field probe data for $h = 12.7$ µm.

This leads to a new design where the height of the radiator will be increased, as was illustrate in section 5.2, in order to decrease the radiated Q-factor. For the modified optimization the height will be increased to be 0.002 inches, or 2 mil. Once again this height is chosen as it is readily available from multiple vendors. The new simulation parameters are displayed in Table 6.3.

Table 6.3. Final optimized SwO physical geometry.

SwO Physical Dimension	Microns (µm)
Substrate Height, h	50.4
Antenna Length, l_a	$\lambda / (2\sqrt{\varepsilon_r}) = 200$
Antenna Width, w	$\lambda / (8\sqrt{\varepsilon_r}) = 50$
Switch Length, l_s	10
Thickness of SwO	1
Thickness of Ground Plane	1
Substrate and Ground Plane Length	$3\lambda = 1200$
Substrate and Ground Plane Width	$3\lambda = 1200$

The key results for this simulation are shown in Table 6.4.

Table 6.4. Final optimized SwO performance summary.

SwO Performance Characteristic	Simulated Value
Resonant Frequency	0.4153 GHz
Q-Factor	16.987
E_{max} (V/m)	24.542 V/m

The electric far field probe data is shown below in Figure 6.3. In this design the radiated Q-factor is much lower, leading to a period of ~70 ps for the stored energy to be radiated.
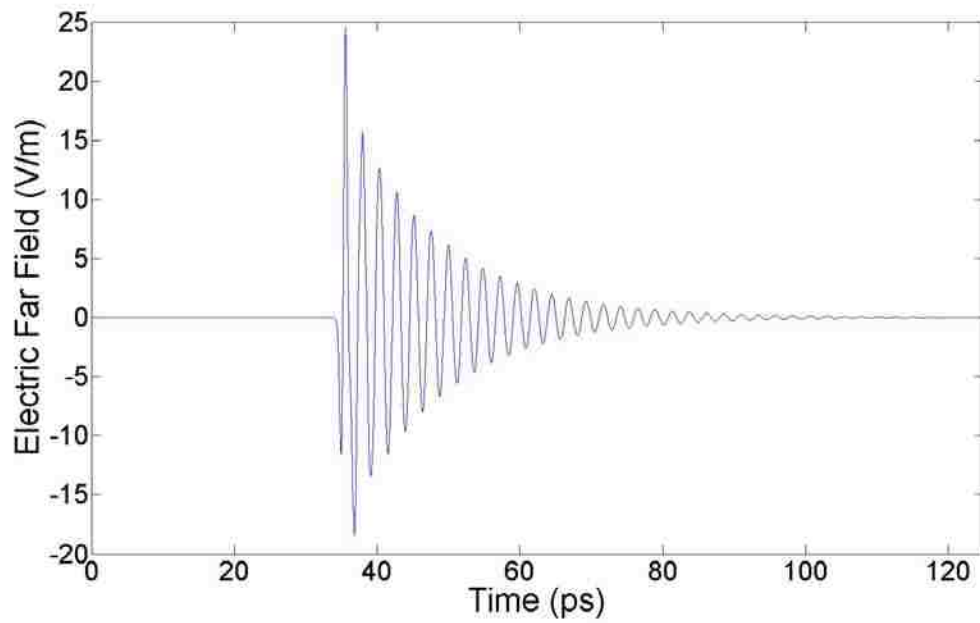
Figure 6.3. Electric far filed probe data for $h = 50.4$ µm.

The data still has a narrow band emission as is shown in Figure 6.4.

The Q-Factor is: 16.9886
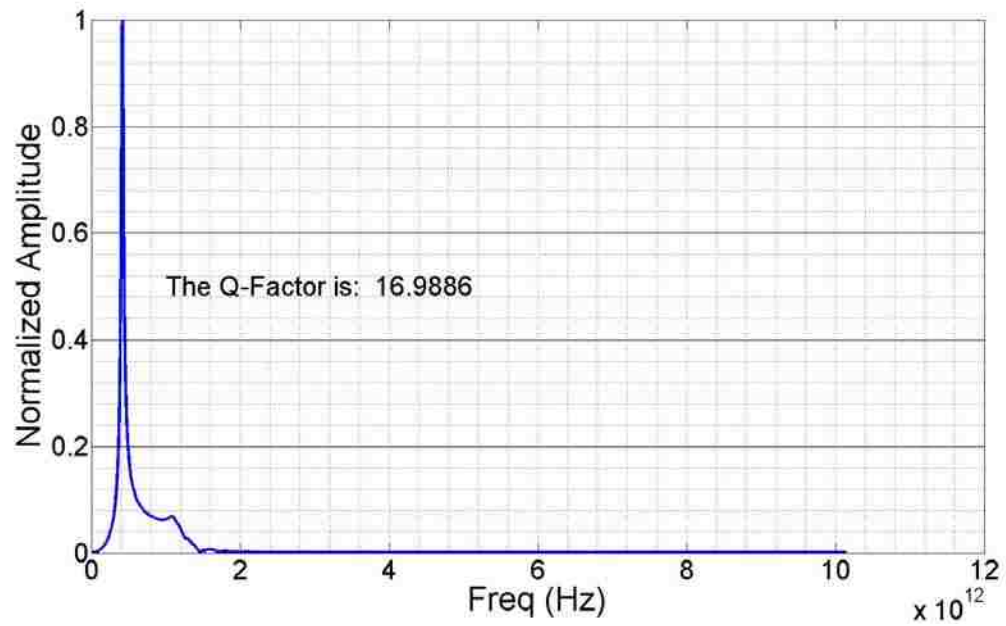
Figure 6.4. Electric far field spectral emmission for $h = 50.4$ µm.

The radiation pattern from the device is plotted and shown to be dipolar in Figure 6.5.

Directivity Abs (Theta=90)

farfield (f=0.4153) [1]

Frequency = 0.4153
Main lobe magnitude = 2.6 dBi
Main lobe direction = 270.0 deg.
Angular width (3 dB) = 98.2 deg.

Phi / Degree vs. dBi
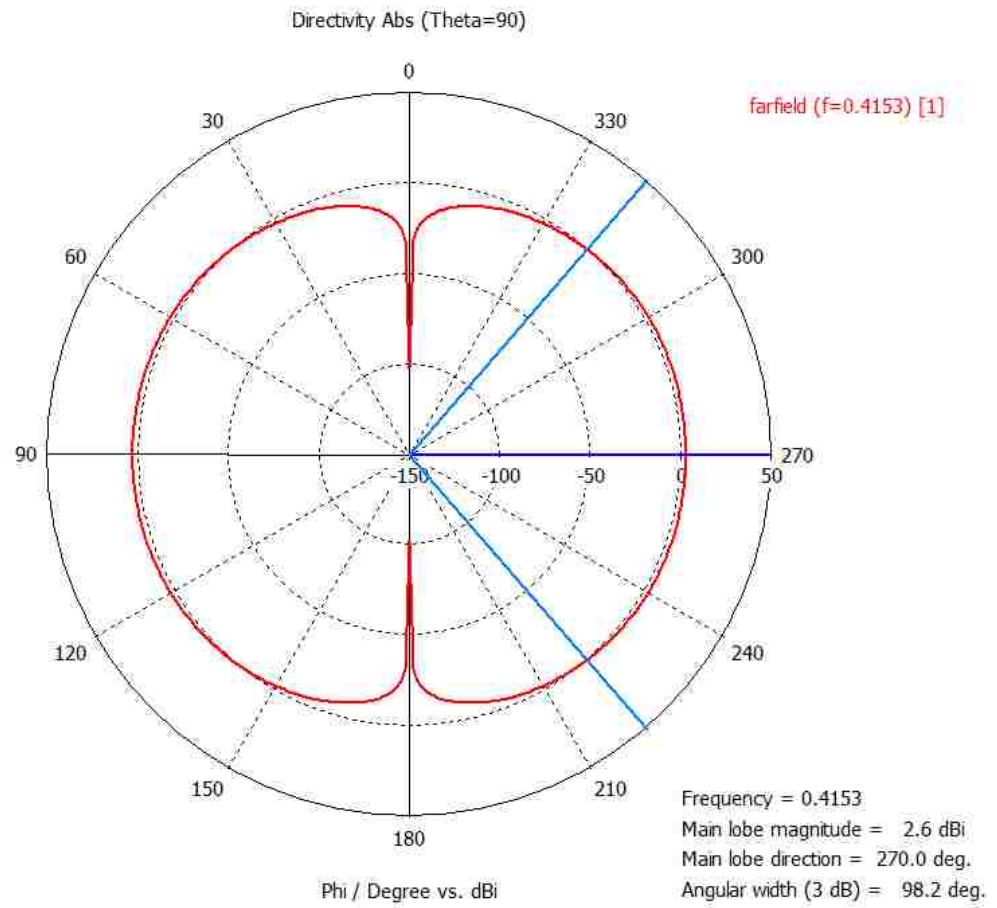
Figure 6.5. Final optimized SwO radiation pattern.

Lastly, the 3D image of the radiated directivity is shown in Figure 6.6.

72

Type	Farfield
Approximation	enabled (kR >> 1)
Monitor	farfield (f=0.415) [1]
Component	Abs
Output	Directivity
Frequency	0.415
Dir.	6.249 dBi
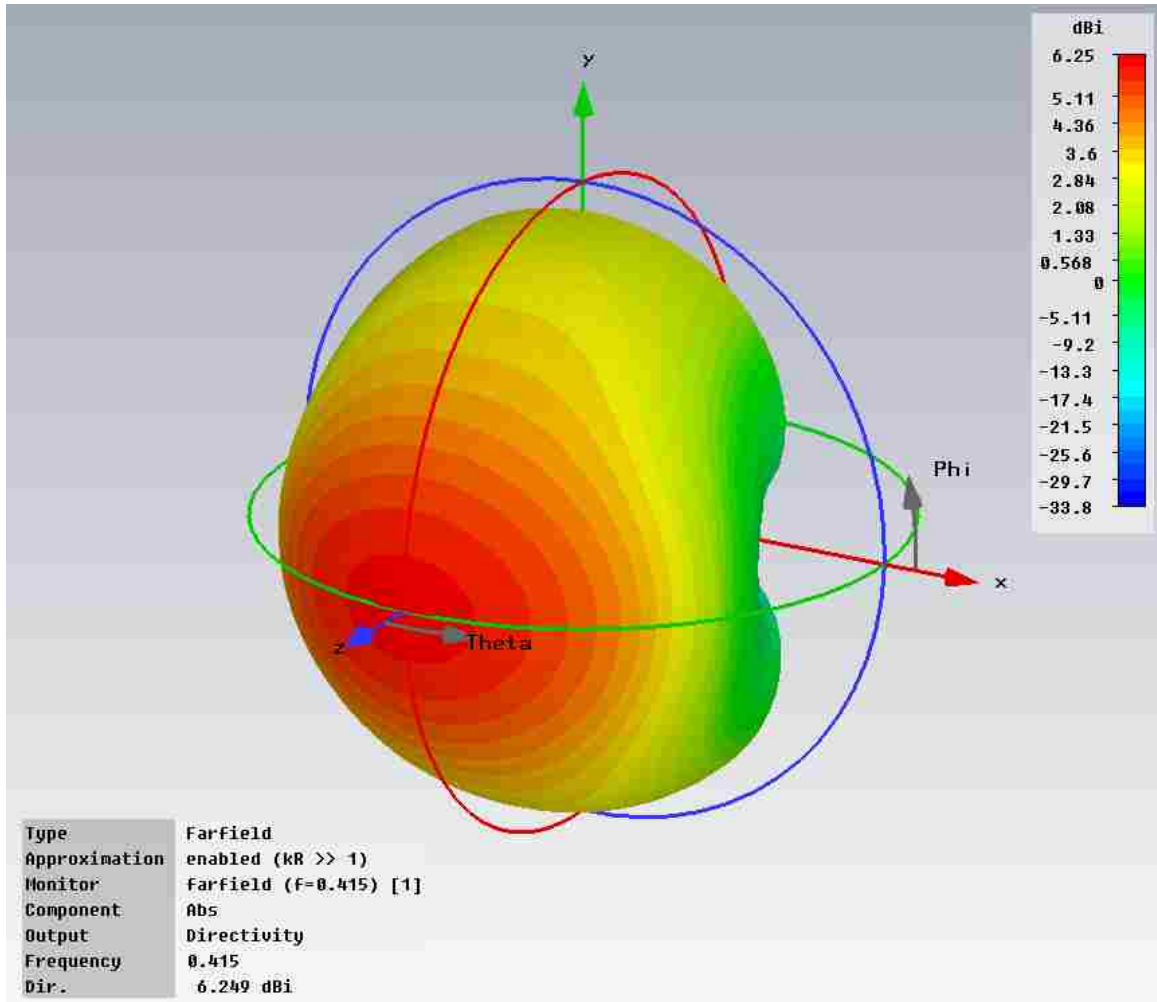
Figure 6.6. Final optimized SwO 3D radiation pattern.

These results illustrate the overall simulated performance for the final optimized SwO. This design geometry, with values as stated in Table 6.2, is the recommended test setup; around which physical experimentation at UTOL may be designed. The simulated performance of the SwO documented in this chapter will then be used to set up metrics for comparison to the experimental data. After measured physical performance results are available they can be compared against the simulated behavior. Comparison of simulation and experimentation is necessary to verify the conclusions reached herein, and results of both are needed to optimize the design for the array of SwO.

Chapter 7

Conclusions

By successfully simulating the experimental conditions at UTOL and duplicating the experimental results in simulation the method used to optimize the SwO is validated. The confidence gained from this approach has allowed a fundamental study for the comparison of the SwO to analytical results where the simulation domain and excitation for the SwO are both shown to be correct. Building upon these achievements in simulation, every design parameter is able to be systematically varied for the purpose of fundamental understanding and optimization. The final simulated results presented in chapter 7 show a SwO antenna design that is optimized in simulation that is ready to be physically fabricated and tested against the developed model.

Future Work

This thesis has presented a unique approach to the design of a THz radiator. While many ideas and approaches were considered in this design the choice of focusing on SwO

optimization was made as its presents unique advantages over other THz radiator designs. Previous THz radiator design optimization studies offer a proven approach for the development of the SwO. The simulation approach allows the various parameters of the SwO to be studied independently for optimization with a fair amount of confidence in the validity of combining the individual pieces in a way that optimizes the system. Final conclusions have been drawn from the optimization of the various parameters of the SwO and have been presented.

Even with a successful optimization of the SwO itself, there are many details that are necessary to work through in order to make the SwO THz radiating system a reality. There are issues with the overall triggering of the system as well as fabrication of the structure and even biasing the device. Each case represents a challenge that needs to be overcome for the SwO to become a physical reality.

7.1 Realistic Photoconductive Switch Analysis

The switch that has been simulated in the development of the SwO has been selected to be an ideal switch. This approach was chosen as it has been shown in simulation to reproduce experimental data from UTOL with exceptional accuracy. For the SwO it has been assumed that the input voltage to the device will be representative of a step input as each rectangular plate is charged to opposite potentials with the photoconductive switch then electrically shorting out the two radiating plates.

To a first order, a unit step input does capture the potential difference across the switch gap. However, the resistivity of the switch is time varying with respect to the laser energy used to excite the switch and the photo carrier lifetime of the switch material itself. As the results for each simulation are directly dependent on the photoconductive switch at the center of the design, for the SwO a more accurate model for the switch will create an accurate input excitation that can complete the total model for the THz transmission system. The late time resistance of the switch may have consequential

results for the late time radiation characteristics of the SwO for design with high Q, and this needs to be understood in the final design.

Having a model for the photoconductive switch will also allow the laser energy used to excite the SwO to be optimized for the switch material. Knowing how much laser energy that each SwO requires to be optimally triggered will complete the modeling for the initial THz transmitter, provide more accurate simulation results, and increase confidence in the simulations' ability to predict the real world performance.

7.2 High Voltage Breakdown Across the Switch Gap

The energy stored in the SwO is that of a parallel plate capacitor with the overall dimensions of the radiating elements. The simple relationship used for the energy stored in a capacitor can be directly applied to the SwO antenna configuration. In other words the standard energy calculation of $E=\frac{1}{2}CV^2$ Can be rewritten as:

$$E = \frac{\varepsilon w(l_a - l_s)}{h} V^2 \qquad (7.1)$$

Where E is the energy stored, V is the charge voltage between the radiating elements and the ground plane, and the dimensions are as labeled in Figure 4.2.

Understanding the maximum charge voltage that can be attained at the various switch gap lengths can in turn further optimize the SwO. The energy stored in each element increases as the square of the charge voltage. A longer switch gap allowing twice the charge voltage can lead to nearly four times the stored energy in the SwO. This relationship can be used to further develop the parameters that were found by varying the switch gap length as the longer gap lengths also translate into higher stored energies. This will allow the study for optimizing the radiation characteristics of the switch gap to go one dimension further in that of stored energy vs. switch gap length.

7.3   Dielectrics Above the Switched Oscillator

Placing a dielectric layer above the SwO may allow the building of a quarter wave transformer on top of the radiator. This is practical because the SwO is in effect a narrow band radiator.   For this approach it is critical that the effective permittivity of the substrate be known with the effects of fringe fields around the SwO as it is the effective impedance that is formed within the substrate of the SwO that will allow a matching layer to be designed. The square root of the effective relative permittivity will form a quarter wave transformer to be formed as it is built at a thickness of one quarter of the wavelength in the top dielectric.

The cost of the quarter wave dielectric matching layer is that a solution to focusing the laser through the dielectric matching layer must be found.   It may be possible to simply leave a void where the laser energy is focused but that leads directly to a manufacturing challenge that must be overcome. The same challenge would present itself for the application of a dielectric lens; the intent of the lens would be to better gather and focus the radiation from the SwO.

7.4   Arrays of Switched Oscillator Antennas

The general relationship for element spacing for the SwO array is understood as each SwO can be approximated as a dipole antenna. However the simulation domain may be expanded to include multiple oscillators so that fringe and coupling effects of the entire array may be analyzed. Simulating an array of antennas can also assist in analyzing tertiary scattering effects between elements and much broader ground planes.

Biasing the array of SwOs may yield challenges as the standoff distances that are needed for the SwO will have to be replicated on the bias lines for all of the radiating elements. The biasing lines are designed to be more resistive than the SwO and any bend

in the trace will lead to parasitic inductance. These features may lead to better isolation of the SwO from the biasing source but can also lead to longer charge times for the SwO. As such this will have to be explored and understood because the charge time for the array of SwO will be a determining factor in how often the array may be pulsed in repetition.

7.5 Fabrication of the Switched Oscillator Antennas

Actually growing the substrate that will be used as the photoconductive switch for the SwO and mating the radiating elements to the switch will yield new elements that have to be brought into the simulation domain. Build tolerances may lead to the spectral emission of the overall array being slightly broader than that of a single SwO. It may also lead to further optimization as values for the radiated power density have clear peaks at specific geometries.

It is intended that the SwO be fabricated on polyethylene for its dielectric properties. Contrasting to previous THz radiator designs, the radiating elements have used etch or CVD techniques to build the radiators on the photoconductive switch itself. In this case polyethylene is not a photoconductive material so mating the polyethylene to the photoconductive switch presents a challenge in its fabrication.

Simultaneous laser initiation of multiple SwO also represents a significant design challenge. First, each switch gap requires that laser energy be directly focused on each gap. Then, acquiring the temporal precision needed such that the entire array is illuminated concurrently will require design effort.

7.5.1 Etching Around Dielectric Surface Waves

Building the SwO may allow fabrication solutions to recurring challenges in the design itself. Dielectric surface waves are a concern in the design of the SwO as they direct energy away from being radiated as intended. Using the etch process that grows the substrate it may be possible to surround each SwO with a conducting shell. This condition does not allow the transmission of dielectric surface waves and as such reflects the wave front back to the SwO. Another solution may be to etch away the substrate material to provide a groove around the SwO creating a discontinuous surface to reject the propagation of the dielectric wave. It may also be possible to etch away most of the surrounding dielectric around the SwO entirely. Dielectric surface waves do not pose a concern if there is no dielectric for the wave to propagate along. However none of these questions can be answered via simulation.

7.6   Experimentally Testing the Switched Oscillator Antenna

While every attempt has been made to faithfully represent the SwO in a simulated space, there is no simulation that can provide the same information as a real experiment. Fabricating the SwO and testing its performance against the simulated and analytically derived results is a very necessary step in its design development. After the experiment the results may be directly compared to predicted values and further optimization may be made.

References

[1] National Telecommunications and Information Administration. *U.S. Frequency Allocation Chart.* http://www.ntia.doc.gov/osmhome/osmhome.html (accessed September 4, 2010).

[2] Ultrafast Terahertz Research Group. *Goal Statment.* http://utol.ecen.ceat.okstate.edu/goal.htm.

[3] Shur, Michael. "Terahertz Technology: Devices and Applications." *Proceedings of ESSCIRC.* Grenoble, France, 2005.

[4] C. Jastrow, S. Priebe, B. Spitschan, J. Hartmann, M. Jacob, T. Kurner, T. Schrader, and T. Kleine-Ostmann. "Wireless Digital Data Transmission at 300GHz." *Electronics Letters*, April 29th, 2010: Vol. 46. No. 9.

[5] Sakai, K. *Terahertz Optoelectronics.* Heidelberg, Germany: Springer, 2005.

[6] C. Jastrow, K. Munter, R. Piesiewicz, T. Kurner, M. Kock and T. Kleine-Ostmann. "300 GHz Transmission System." *Electronics Letters*, January 31st, 2008: Vol. 44 No. 3.

[7] R.T. Kinasewitz, B. Senitzky. "Investigation of the Complex Permittivity of n-type Silicon at Millimeter Wavelengths." *Journal of Applied Physics, Vol. 54*, 1983: 3394-3398.

[8]   Baum, Carl. "Sensor and Simulation Note 541 - 542, Theoretical Note 285,." *Summa Foundatation.* 2010. http://www.ece.unm.edu/summa/notes/index.html.

[9]   Allen Taflove, Susan Hagness. *Computational Electrodynamics.* Norwood, MA: Artech House, INC, 2005.

[10] N. Katzenellenbogen, Hoi Chan, D. Grischkowsky. "New Performance Limits of an Ultrafast THz Photoconductive Receiver." *OSA Proceedings on Ultrafast Electrinics and Optoelectronics*, 1993: 123-125.

[11] Katzenellobogen, D. Grischkowsky and N. "Femtosecond Pulses of Terahertz Radiation: Physics and Applications." *OSA Proceedings on Picosecond Electronics and Optoelectronics*, 1991: 9-14.

[12] F.E. Doany, D. Grischkowsky, and C.- C. Chi. "Carrier Lifetime Versus Ion Implantation Dose in Silicon on Sapphire." *Applied Physics Letters, Vol. 50*, 1987: 460-462.

[13] Serway, Beichner. *Physics for Scientists and Engineers 5th Edition.* Orlando, FL: Saunders College Publishing, 2000.

[14] P. Kumar, C. E. Baum *Maximizing Energy in Terahertz Pulse Radiation from a Switched Oscillator.* Summa Foundation, 2010.

[15] McMillan, R. W. "Terahertz Imaging, Millimeter-Wave Radar." In *Advances in Sensing with Security Applications*, by J. Byrnes, 1-26. Huntsville, Alabama USA: Springer, 2006.

[16] C. E. Baum, P. Kumar, S. Altunc, K. McDonald, C. G. Christodoulou, and E. Schamiloglu. *Choice of Frequencies for THz Atmospheric Transmission.* Summa Foundation, 2009.

[17] Pozar, David. "Microstrip Antennas." *Proceedings of the IEEE*, 1992: Vol. 80, No. 1 79-91.